Utrecht University

Master's Thesis - Water Science and Management

The importance and vulnerability of the Indus regional Water Towers

-Applying the global Water Tower Index at subbasin scale-

Wolledge (2012)

Esmée Mikayla Mes
5885604

Supervision
Prof. dr. Walter Immerzeel – Utrecht University, Faculty of Geosciences
Dr. Arthur Lutz– Utrecht University, Faculty of Geosciences

June 24, 2021

Summary

Mountains occupy a critical role in the storage and supply of sufficient freshwater to livelihoods and ecosystems in lowland areas. This role is further emphasized by the term 'water towers'. According to the global Water Tower Index (WTI) developed by Immerzeel et al. (2020), the most important water tower globally is the Indus Basin, where the water provisioning role of the mountains to the dry lowlands is especially large. Their Vulnerability Index (VI) additionally displayed the vulnerability of the Indus water tower to several indicators. The global scale of the study, however, prevented both the ability to draw conclusions on a scale smaller than the entire Indus Basin as well as the use of regional data. It is therefore unclear where the most important and vulnerable regions within the Indus Basin are located. Additionally, it is unclear whether a more regional approach would show larger spatial variety compared to the global WTI within the Indus Basin and whether it could potentially function as a first estimate and orientation tool for more complex and time-intensive hydrological studies.

Here, I apply the WTI and VI at subbasin scale for the Indus Basin to determine whether these are applicable at subbasin scale. This new approach is termed the regional Water Tower Index (rWTI), where a Supply Index (SI) and Demand Index (DI) are determined through several indicators. The VI consists of static and dynamic indicators, including government effectiveness, hydro-political tension, water stress, climate changes, and socio-economic changes. Eight delineated regional Water Tower Units (rWTU) are ranked by their importance and vulnerability using both global and regional data. The use of global data at subbasin scale enables a comparison to the findings by Immerzeel et al. (2020), while outcomes derived through regional data are compared to findings derived by more complex hydrological studies.

I conclude that the global WTI and VI are applicable at subbasin scale. Application of global data in the Indus subbasins already shows large variability in outcomes between the rWTUs and the Indus Water Tower Unit (WTU), showing that the global WTI-approach does not sufficiently consider the regional variety. The use of regional data changes the outcomes for all indicators, thereby improving the representation of spatial variability compared to global scale assessments, especially for the glacier indicator, snow indicator and the DI. Findings agree well with other studies, further demonstrating the applicability of the global WTI and VI at subbasin scale.

The applicability of the rWTI in other river basins could provide further evidence on whether the regional approach can function as an estimate and orientation tool for complex hydrological studies, although this study gives the first indication that it can. Beas/Sutlej is found to be the highest scoring rWTU, both due to having the second highest SI and having the highest DI, indicating it is the most important rWTU within the Indus Basin. This research could therefore be most useful for local political parties, inhabitants, tourists, and farmers of Beas/Sutlej and could be crucial in raising awareness on its importance and vulnerability.

Acknowledgements

I want to offer my gratitude and appreciation to dr. Arthur Lutz and prof. dr. Walter Immerzeel for their guidance, help and feedback in writing this thesis. Without their elaborate answers, feedback and provision of datasets, this research would not have been possible. Working through a computer screen has not prevented them from helping me in the best possible way, so thank you. It has been a privilege to have worked with the both of you.

I would also like to thank Femke van Woesik and Chris Larrea for their support during the long library days and the motivation they have given me. Thank you for pushing me to always work harder and provide an even better result, but also to remind me that taking breaks is a necessity.

Finally, I would like to express my gratitude to the researchers who have made the datasets available. I have used many different datasets during this research, of which some were still under review. Without these datasets, I would not have been able to finish this thesis, therefore I am truly grateful.

Table of contents

Table of figures

Table of tables

1. Introduction

Mountains are important as these redistribute winter precipitation to spring and summer discharge and reduce the intra-annual variability of river flows (Vivroli et al., 2011). Additionally, mountains generate approximately twice as much runoff compared to the lowlands, which can be seven times as high in arid areas (Immerzeel et al., 2020; Hock et al., 2019; Huss et al., 2017; Viviroli et al., 2009; Messerli et al., 2004). Mountains further host cultural sites, attract tourists, and have high biodiversity (Immerzeel, 2020; Wang et al., 2019; Viviroli et al., 2011; Hock et al., 2019).

Because of their important hydrological roles, mountains can be classified as 'water towers'. This term emphasizes the importance of mountain ranges in storing and supplying sufficient freshwater to livelihoods and ecosystems in lowland areas (Immerzeel et al., 2020; Viviroli et al., 2007). Hydrological boundaries are the fundament for a water tower unit (WTU), as water supply and demand are linked at river basin scale (Immerzeel et al., 2020). For the visualisation and further explanation of the global WTUs, see Annex I.

According to Immerzeel et al. (2020), the most important water tower globally is the Indus. The Indus WTU consists of high-elevated upstream areas, contains the largest glacial system outside of the polar regions, and has the most extensive snow cover of the Asian basins (Immerzeel et al., 2015). Opposed to this scarcely populated and wet upstream area, lies the arid and densely populated downstream area where over 215 million people rely on the upstream water (Koppes et al., 2015; Bocchiola & Soncini, 2019; Immerzeel et al., 2020). The already large population is projected to grow further to 383-438 million people in 2050, and in combination with urbanization and economic growth puts pressure on the Indus water resources (Laghari et al., 2012; Bocchiola & Soncini, 2019; Wijngaard et al., 2018; Viviroli et al., 2020). The basin might even be more vulnerable to changing water supplies due to climate change (Scott et al., 2019). The melt-characteristics of the Indus cryosphere are changing, thereby altering the timing, volume, and variability of discharge to downstream areas (Immerzeel et al., 2010; Koppes et al., 2015; Messerli et al., 2004). Changes in precipitation patterns occur, further altering glacier volume, snow cover, and runoff characteristics (Wijngaard et al., 2017). The basin is additionally vulnerable to hydro-political tensions, due to upstream infrastructure constructions in its transboundary rivers, and water stress, due to unsustainable groundwater extractions (Cheema & Qamar, 2019; Archer et al., 2010; Immerzeel et al., 2020).

Besides the research of Immerzeel et al. (2020), Viviroli et al. (2007) also assessed water towers globally based on mountain typology and found that for the Indus Basin most discharge in the lowlands originates from the mountains. The global scale of these studies, however, prevented both the ability to draw conclusions on a scale smaller than the Indus Basin as well as the use of regional data. Uncertainty therefore remains on where the most important and vulnerable regions within the Indus Basin are located. Other research that has been done on the regional scale for the Indus Basin has largely focused

on separate components of the hydrological cycle instead of the total water balance. Several studies have assessed the cryosphere aspect, such as Koppes et al. (2015), who found that the current glacier runoff contributes between 4-78% to the total annual Indus discharge, and Biemans et al. (2019), who found that snowmelt and glacial melt still contribute 60-70% to the Indus discharge at the outlet into the Arabian Sea. Immerzeel et al. (2015) focused on determining the precipitation in the Upper Indus Basin (UIB) and found that high-altitude precipitation can be 2-10 times higher than was previously determined. Several studies researched the contributions of the different hydrological processes and sources to runoff in the Indus Basin. Lutz et al. (2014) found that the Indus runoff is a varied mix of different sources and that the annual runoff between 2041-2050 will likely increase by 7-12% compared to 1998-2007. Subsequently, Lutz et al. (2016) found that water availability changes for 2071-2100 will vary between -15% and +60% compared to 1971-2000. It is evident from these studies that there is a large focus on climate change, and how this alters the hydrological processes in the Indus Basin. However, population growth, economic growth, water stress, and hydro-political factors are changing the supply and demand as well. Wijngaard et al. (2018) found that the combined effect of climate and socio-economic changes would alter the annual water gap by -21% to +7% between 2071-2100 compared to 1981-2010. Finally, Viviroli et al. (2020) found a population increase from 44 million in 1960 to 210 million in 2040 and that 92-95% of the Indus population depends on mountain runoff.

What is evident from this overview is the lack of an integrated view of all contributions to the water supply and demand, both currently and in the future, at a scale smaller than the WTU. Immerzeel et al. (2020) did make a consistent framework to assess and rank the importance and vulnerability of WTUs, however it is unclear whether a more regional approach would show larger spatial variability compared to the global WTI. Additionally, other studies that have focused on modelling regional hydrological processes in the Indus Basin through detailed hydrological models are data-intensive and time-consuming (Viviroli et al., 2020; Biemans et al., 2019), while a more regional approach to the WTI could potentially lead to similar conclusions for the region in a faster and less-complex manner.

This research accordingly aims to develop an integrated framework of the contributions to water supply and demand on a subbasin scale to assess whether taking a regional Water Tower Index (rWTI) approach provides different results and improved representation of spatial variability compared to global scale assessments. It thereby aims to determine where the most important and vulnerable regions within the Indus Basin are located for two reasons. First, these results can provide evidence on whether the regional approach can potentially function as a first estimate and orientation tool to the data-intensive and time-consuming hydrological studies. Second, these results are useful for people living and working in the subbasins as well as for tourists, thereby contributing to society. Moreover, the basin is a large food exporter and plays an important role in maintaining global food security (Cheema & Qamar, 2019). It is therefore important to raise awareness about the importance and vulnerability of the Indus Basin to people globally.

To determine the importance and vulnerability of the mountain ranges in the Indus subbasins, the global Water Tower Index (WTI) approach of Immerzeel et al. (2020) is followed, but with higher spatial detail and using regional datasets. This entails the calculation of a Supply Index and Demand Index, which together form the WTI. These WTI-values then indicate the importance of the different regional water tower units (rWTUs) in the Indus Basin. This is followed by the calculation of a Vulnerability Index, in which the subbasins' vulnerability is assessed. Following this approach, the use of both global and regional data will ultimately prove whether the WTI-approach is applicable at subbasin scale. The main research question is therefore as follows:

To what extent are the global Water Tower Index and Vulnerability Index applicable at subbasin scale?

This research question is answered based on the following sub-questions:

1. Does application of the Water Tower Index at subbasin scale provide better representation of spatial variability in the Water Tower Index and the Vulnerability Index within a river basin?
2. Does the use of regional data over global data change the Water Tower Index and Vulnerability Index calculation results?
3. How do conclusions drawn from the application of the Water Tower Index and Vulnerability Index at subbasin scale differ from conclusions drawn in hydrological modelling studies at the same scale?

2. Theory

Theoretical insights into the study area, the global WTI and the rWTI are required to answer the sub-questions. Therefore, the study area is discussed, followed by an explanation of the global WTI and the outcomes found by Immerzeel et al. (2020) for the Indus Basin. Subsequently, the different supply indicators and their underlying processes, such as the snow-albedo feedback for the snow indicator, are described. This is followed by discussing where the demand indicators are highest within the Indus Basin and why. Lastly, projections of the dynamic vulnerability indicators are given and the roles of the static indicators within the Indus Basin are discussed.

2.1. The study area

The Indus Basin is a river basin located in South Asia (Figure 1), overlying Pakistan, China, India, and Afghanistan (Bocchiola & Soncini, 2019; Bolch, 2019). The basin covers an area of 863,508 km^2, whereas the upstream basin, or Upper Indus Basin (UIB), consists of a drainage area of approximately 164,860 km^2 (Amin et al., 2018; Khan et al., 2014). The Indus Basin contains the largest glacial system outside of the polar regions (Immerzeel et al., 2015), causing glacial melt to dominate the Upper Indus runoff composition regimes by 40.6% (Wijngaard et al., 2017; Bocchiola & Soncini, 2019). The snow-covered area is even a magnitude greater (Archer et al., 2010). The most important river in the basin is the Indus River accompanied by its tributaries, amongst which the most significant are Jhelum, Chenab, Sutlej, Ravi, and Beas. These rivers flow from the Hindu Kush, Karakoram, and Himalayan (HKH) mountain ranges to the Arabian Sea (Archer et al., 2010; Bocchiola & Soncini, 2019; Shrestha et al., 2019, Mesquita et al., 2019).

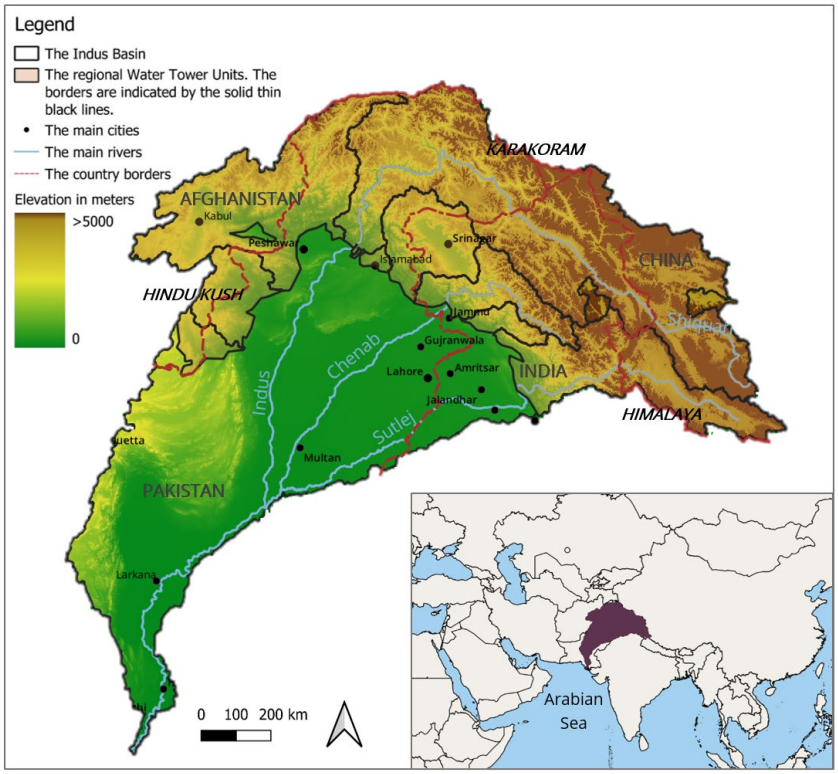

Figure 1: Map of the Indus Basin.

The Indus Basin is heterogenic in both topography and climate (Bolch et al., 2019), where the overall climate varies from subtropical-arid to subhumid to alpine and the average temperature varies from 2˚C to 49˚C (Shrestha et al., 2019; Amin et al., 2018). The mean evaporation of 1650-2040mm classifies the basin as semi-arid to arid. The annual rainfall variability is large, amounting to 90-500mm in downstream areas, while reaching up to 3000mm in the UIB (Shrestha et al., 2019; Immerzeel et al., 2015). The intra-annual precipitation variability is additionally large, as there is a bimodal distribution due to the westerlies and summer monsoon (Shrestha et al., 2019). The monsoon intrusion is, however, limited by the mountain ranges, causing most precipitation to fall during the westerlies (Bocchiola & Soncini, 2019).

2.2 The global Water Tower Index

The global WTI is an index on river basin scale developed by Immerzeel et al. (2020). The WTI consists of a Supply Index (SI) and Demand Index (DI), which together indicate how important each WTU is in providing sufficient mountainous water to hydrologically connected downstream areas. The WTI is high if a mountain range contains abundant water resources, and if that water is in great demand downstream. The SI consists of four indicators: (1)precipitation, (2)surface waters, consisting of lakes and reservoirs, (3)glaciers, and (4)snow. The DI consists of four indicators: (1)irrigation demand, (2)industrial demand, (3)domestic demand, and (4)the environmental flow requirement. Immerzeel et al. (2020) also explore vulnerabilities of the different basins, which are either static or dynamic. The static vulnerabilities comprise of (1)water stress, indicated by baseline water stress (BWS), (2)government effectiveness (GE), and (3)risk for hydro-political tension. The dynamic vulnerabilities consist of (1)climate changes, indicated by precipitation and temperature changes, and (2)socio-economic changes, indicated by population and GDP changes.

2.2.1. Water Tower Index results for the Indus

Immerzeel et al. (2020) presented several findings on the Indus Basin. First, the Indus WTU consists of a balanced mix of precipitation, glacial melt, snowmelt, and surface waters and has an important supplying role. This becomes evident from the SI-value of 0.29 (Figure 2a), which is the second highest value in Asia and Oceania. The DI-value of the Indus Basin amounts to 0.76 (Figure 2a), which is again the second highest value of Asia and Oceania. This is due to the high downstream demand, which cannot be met by the mountainous water supply and the water generated downstream. This SI-value and DI-value are multiplied to form the WTI-value of 0.22. When this WTI-value is normalized compared to the maximum WTI-value found globally, it results in a normalized WTI of 1.00 ±0.03 for the Indus WTU (Figure 2b). This indicates it is globally the most important WTU. The basin was also found to be vulnerable (Figure 2b) to several indicators. Its highest vulnerability is to socio-economic changes, where the population is projected to increase by 50% and the GDP is projected to increase by 769% in

2050 compared to 2016. The Indus Basin is also highly vulnerable to weak GE, as the maximum global vulnerability is set at -1.5 and the basin scores a weak -0.36. The basin is only moderately vulnerable to hydro-political risk (3), as this risk ranges from 1 to 5. Its vulnerability to climate change is low, where a temperature increase of 1.8K is found between 2000 and 2050, while precipitation is even found to increase by 1.4%. The basin's vulnerability to water stress is low (BWS=2.2), which globally ranges from 0 to 5. This low BWS indicates low competition between the different water users in a subbasin.

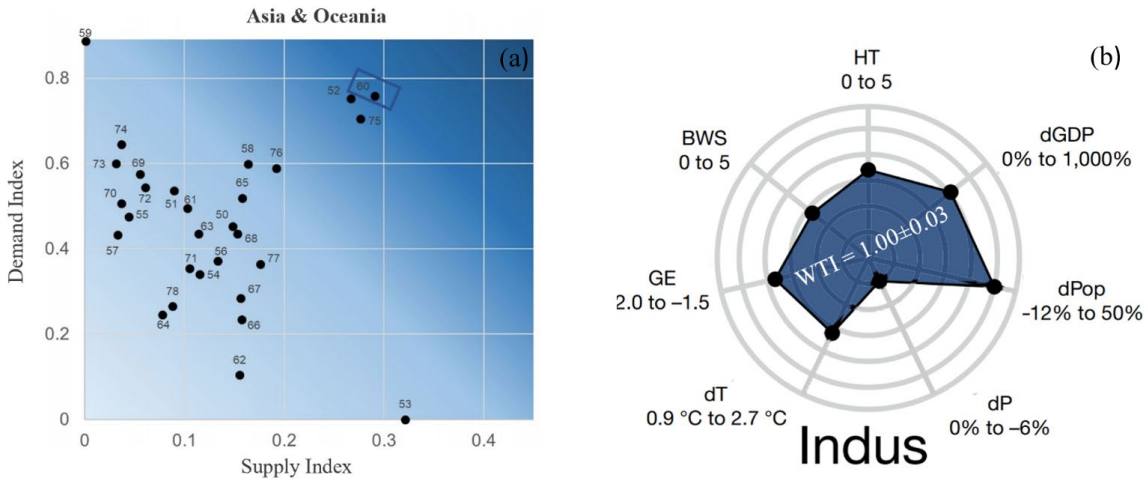

Figure 2: a) Placement of the Indus Basin in Asia and Oceania based on its SI and DI and b) Vulnerability of the Indus Basin (Adapted from Immerzeel et al., 2020).

2.3. The regional WTI for the Indus Basin

The rWTI will, similarly to the global WTI, consist of a SI and DI, of which the values are determined by the regional hydrological processes in the Indus Basin.

2.3.1. Supply Index

The SI comprises four indicators, coinciding with the hydrological regimes within the Indus Basin (Archer et al., 2010). These indicators are precipitation, snow, glaciers, and surface waters.

2.3.1.1. Precipitation

Precipitation in the Indus Basin occurs due to convective and orographic processes, which are both vital in inducing precipitation during the South-Asian monsoon and westerly disturbances (Houze Jr et al., 2007; Medina et al., 2010).

Convective precipitation occurs due to surface heating, causing atmospheric instability, which accelerates the vertical uplift of an air parcel. If the parcel contains sufficient moisture to reach its dewpoint, condensation follows, causing precipitation. Orographic precipitation links to convective precipitation and occurs due to the orographic uplift of a horizontally moving air parcel after encountering a barrier (Dingman, 2015). The steep and high topography in the Indus Basin causes fast

cloud formation, followed by short and intense precipitation (Bolch et al., 2019). Precipitation intensity in the basin therefore shows a strong north-south gradient (Scott et al., 2019).

The South-Asian monsoon delivers the bulk of precipitation between June and September (Bolch, 2019) in the Indus Basin. The interaction between the monsoon and the basin topography causes the effect of the monsoon to fade in northwest direction (Shah et al., 2020; Houze Jr et al., 2007). Convection plays an important role in the precipitation-bringing processes of the monsoon where moisture flows in from the Arabian Sea and Bay of Bengal (Medina et al., 2010).

Westerly disturbances or westerlies are eastward moving cyclones, which cause more than two-thirds of the annual precipitation in the northwest to fall during winter and spring. This amount is, however, still largely influenced by altitude (Bocchiola & Soncini, 2019; Wang et al., 2019; Immerzeel et al., 2015). The disturbances occur due to the blowing of a baroclinic wave towards the Himalaya. The formation of a cold front causes the upwards advection of moisture along the front, which is further uplifted by orographic effects (Cannon et al., 2016).

2.3.1.2. Snow

In the Indus WTU, snowmelt contributes largely to river flows from March to September at elevations over 4000m (Archer et al., 2010; Bolch et al., 2019). The snow cover is largest in early March, amounting to 250,000 km^2 (Immerzeel et al., 2009).

An essential feedback in sustaining the snow cover is the snow-albedo feedback. This feedback entails that snow has a high albedo, thereby reflecting sunlight. When the snow melts, the underlying ground becomes visible, which lowers the albedo and increases the absorption of incoming solar radiation. This leads to further accelerated snowmelt. This process typically occurs annually during spring when higher temperatures decrease the albedo, further amplifying warming (Thackeray et al., 2019).

There are large regions in the UIB where the snow cover persists more than 90% of the time during winter and spring (Immerzeel et al., 2009). There is, however, still a large spatial and temporal variability in snowfall and snow cover (Figure 3) due to steep elevation differences and different atmospheric circulation systems (Dingman, 2015; Bolch et al., 2019). The westerly-affected subbasins in the Indus Basin receive high snowfall and contain large snow cover (51%) as opposed to the monsoon-dominated areas, where the snow cover is limited to high elevations (20%; Bolch et al., 2019; Afzal et al., 2014).

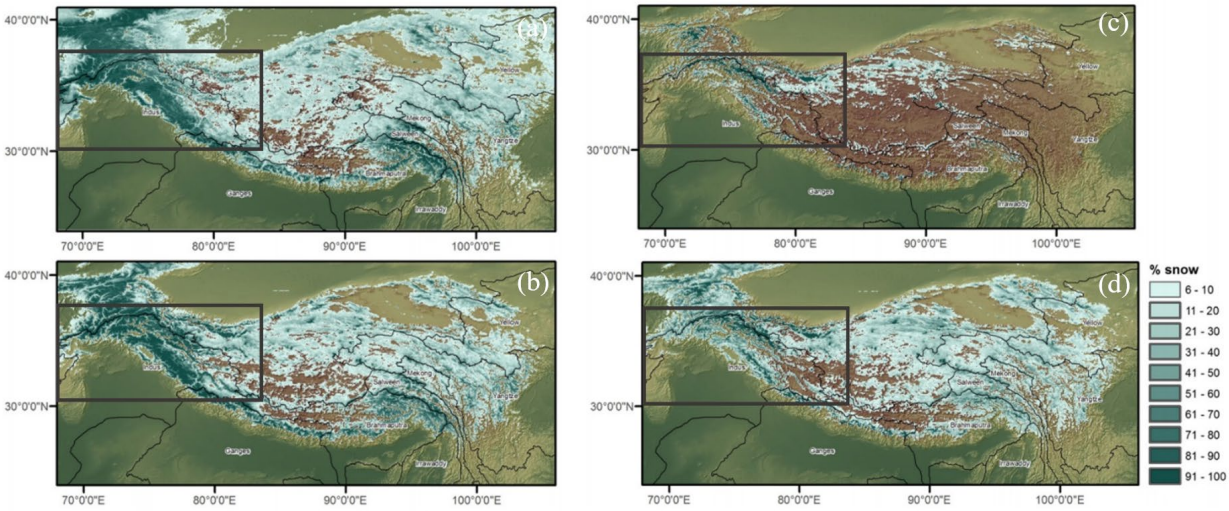

Figure 3: Seasonal snow cover in the Himalaya in a) winter, b) spring, c) summer, and d) autumn. The grey box represents the UIB (Immerzeel et al., 2009).

2.3.1.3. Glaciers

Glaciers store water in ice and are particularly important in supplying water to dry downstream areas, such as in the Indus Basin (Bolch et al., 2019). Glaciers provide a smoothing effect for intra-annual fluctuations in water resources as they especially provide water during spring and summer when river discharges are generally low. Additionally, glaciers provide a smoothing effect for interannual fluctuations by storing water during cold and wet years and releasing it during dry and warm years (Viviroli et al., 2011).

Glacial melt provides about 40% of the Indus runoff (Bolch, 2019; Shah et al., 2020), and the contribution of glaciers is highest upstream. Over 60% of the glaciers in the Indus WTU are located in the Karakoram, 30% in the Himalayas and solely 10% in the Hindu Kush (Bolch, 2019). Even though most glaciers are located in the Karakoram, meltwater generation is not necessarily highest in this region as high-elevated glaciers in the centre of the Karakoram respond differently to climate change (Archer et al., 2010). Many glaciers in this region appear to be stable or are advancing (Mesquita et al., 2019), known as the Karakoram anomaly (Bocchiola & Soncini, 2019; Bolch et al., 2019). The occurrence of these surges is hypothesized to be due to the interplay of the two major atmospheric circulation systems, which decreases the region's temperatures (Lund et al., 2020). Glaciers in the Western Himalaya are losing mass by approximately -0.6 m w.e./year, whilst this is -0.3 m w.e./year for the Hindu Kush (Bolch et al., 2019).

2.3.1.4. Surface waters

Surface waters in the Indus Basin comprise man-made reservoirs, glacial lakes, and non-glacial lakes. The basin contains eight major reservoirs and many smaller reservoirs. These are largely multi-purpose reservoirs for storing and regulating water, generating hydropower, and providing flood control (Cheema & Qamar, 2019; Khan et al., 2017).

Glacial lakes are fed by glacial meltwater and can be located on top of glaciers, in front of glaciers or lie close to the glacier termini (Bolch et al., 2019). The exact number of glacial lakes in the Indus Basin is uncertain but estimates range from 4,260 to 8,200 in the total HKH region, of which the Indus Basin is only a small section (Bolch et al., 2019). Most of the lakes occur within the 4000-4500m elevation range, which coincides with high glacier occurrences (Ashraf et al., 2017).

Non-glacial lakes are solely fed by precipitation and snowmelt and occur less in the Indus Basin, as glacial lakes are over 70% higher in number and lake area (Bolch et al., 2019). Most non-glacial lakes occur between 3500-4000m in the UIB (Ashraf et al., 2017).

Lakes can be endorheic or exorheic; endorheic lakes are lakes where water does not drain from (Zhang et al., 2017). The Tibetan Plateau, a high plateau in southwestern China, overlaps partly with the Indus Basin and comprises of 30,000 lakes of which 434 are endorheic (Li et al., 2019; Liu et al., 2021). It is important to examine whether these lakes lie in the UIB, as these do not contribute to the downstream water supply. These endorheic lakes should therefore be excluded from the surface water indicator, forming an improvement over the global WTI-approach.

2.3.2. Demand Index

The DI comprises four indicators, coinciding with the different sectoral demands: industrial demand, domestic demand, irrigation demand and the environmental flow requirement (EFR). The first three indicators form the human demand (Bocchiola & Soncini, 2019).

The human demand in the Indus Basin is large, amounting to 767 km^3/year, of which the different sectors demand different amounts of water (Table 1). This number entails the total amount of water required for withdrawals and does not include return flows (Wijngaard et al., 2018). The irrigation indicator is the most important as approximately 93%-96% of the Indus Basin's water resources are used for agriculture (Table 1; Cheema & Qamar, 2019). The agricultural sector has expanded largely to meet the world's demand for food and fibre through the world's largest irrigation network called the Indus Basin Irrigation System (IBIS; Archer et al., 2010; Immerzeel et al., 2010). 40% of the agricultural food production is exported, while this is up to 60% for fibre (Laghari et al., 2012; Kiani et al., 2018). Figure 4a displays the irrigation consumption rates within the Indus Basin, which differ from the water demand as these include return flows. However, it can indicate where irrigation consumption and, therefore, likely, the irrigation demand in the Indus Basin is highest. The highest consumption rates of

600 mm/year given over the irrigation croplands occur in the centre and east of the basin (Wijngaard et al., 2018).

Domestic demand and industrial demand are almost neglectable compared to the irrigation demand. The domestic demand is thereby largely fulfilled by (unsustainable) groundwater extractions (Archer et al., 2010; Wijngaard et al., 2018). The domestic and industrial consumption, given in Figure 4b, can again give an indication on where the highest domestic and industrial demand occur. Solely in urban areas does the consumption surpass the 100 mm/year given over the urban area (Figure 4b; Wijngaard et al., 2018).

Additional to the human demand, there is also the EFR (Table 1). The EFR entails the minimum residual flow required to mimic the natural river regime and thereby sustain ecological functions (Archer et al., 2010; Scott et al., 2019). Currently, the EFR and irrigation demand conflict and irrigation needs are already prioritised over the EFR (Wijngaard et al., 2018). In total 83 km^3/year (11% of the total demand in the Indus Basin) is unmet, which is compensated by unsustainable groundwater extractions (Wijngaard et al., 2018).

Table 1: Water demand (km^3) per sector (Wijngaard et al., 2018).

	Total human demand (km^3)	**Irrigation demand (km^3)**	**Domestic demand (km^3)**	**Industrial demand (km^3)**	**Environmental Flow Requirement (m^3/s)**
Demand (km^3)	767	720	37	10	$8x10^3$
Demand (% of total human demand)	100	94	4.8	1.3	Non applicable

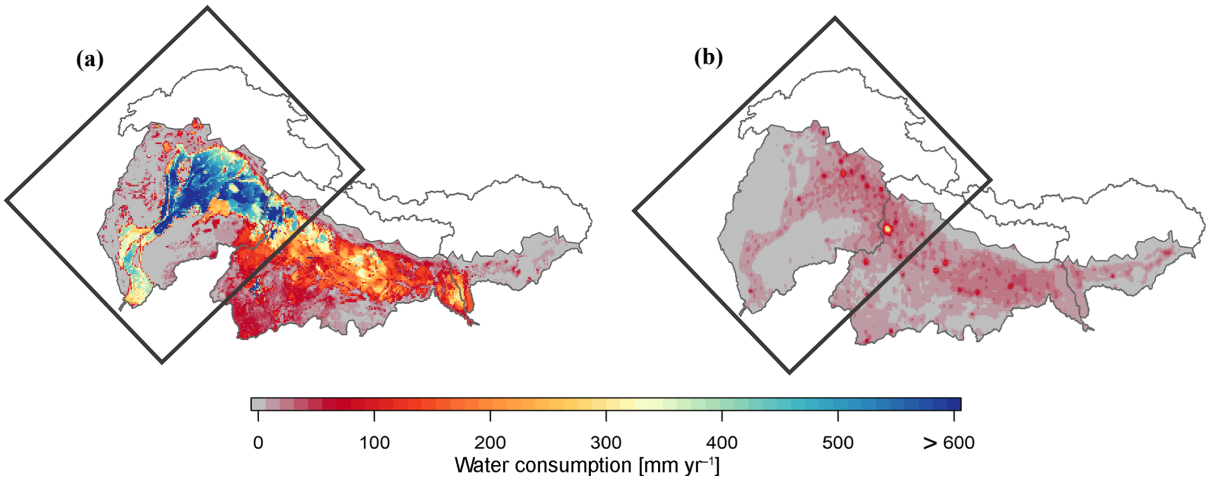

Figure 4: a) The annual irrigation consumption and b) the domestic + industrial consumption. The grey box represents the Indus Basin (Adapted from Wijngaard et al., 2018).

2.3.3. Vulnerability Index

The Indus subbasins and rWTUs are vulnerable to factors that alter water supply and demand. These factors can either be dynamic, such as climate change and socio-economic change, or stagnant, such as hydro-political tension, governmental effectiveness, and water stress.

2.3.3.1. Vulnerability to climate change

Climate change can limit the future water supply through increasing temperatures and decreasing precipitation, thereby increasing the vulnerability of the subbasins.

Temperature changes affect glacial melt and snowmelt, in which elevation-dependent warming (EDW) plays a role. EDW entails the amplified rate of warming at higher elevations, leading to accelerated melt in mountainous areas (Krishnan et al., 2019; Pepin et al., 2015). Figure 5a displays the projected trends for the UIB for RCP4.5 and RCP8.5. RCP4.5 is an intermediate concentration pathway in which radiative forcing stabilizes by 2100, while RCP8.5 is the most extreme concentration pathway containing the highest greenhouse gas emissions. According to both RCPs, the temperature changes are evenly divided over the UIB but are slightly higher in the western subbasins. The dry-warm model shows a more significant increase than the other models, with temperature increases of 9°C for RCP8.5 (Khan & Koch, 2018).

Future precipitation changes are expected to occur due to the intensification of the hydrological cycle. This intensification relates to the Clausius-Clapeyron relation, which dictates that warmer air can hold more water vapor. As evaporation rates will increase due to higher temperatures, more water returns to the atmosphere, which the warmer atmosphere is able to hold. More water is thereby collected, leading to an intensification of the hydrological cycle (Dingman, 2015). The monsoon dynamics are expected to change in the UIB by fewer rainy days, but increased intensity and mean of monsoon precipitation (Wijngaard et al., 2018; Hock et al., 2019). Additionally, more precipitation will fall in the form of rain instead of snow (Bolch et al., 2019). Figure 5b displays the projected precipitation trends for the UIB, where the highest precipitation increase occurs in the east and the highest decrease occurs in the west. The largest spatial variability is found for the dry-warm model (Khan & Koch, 2018).

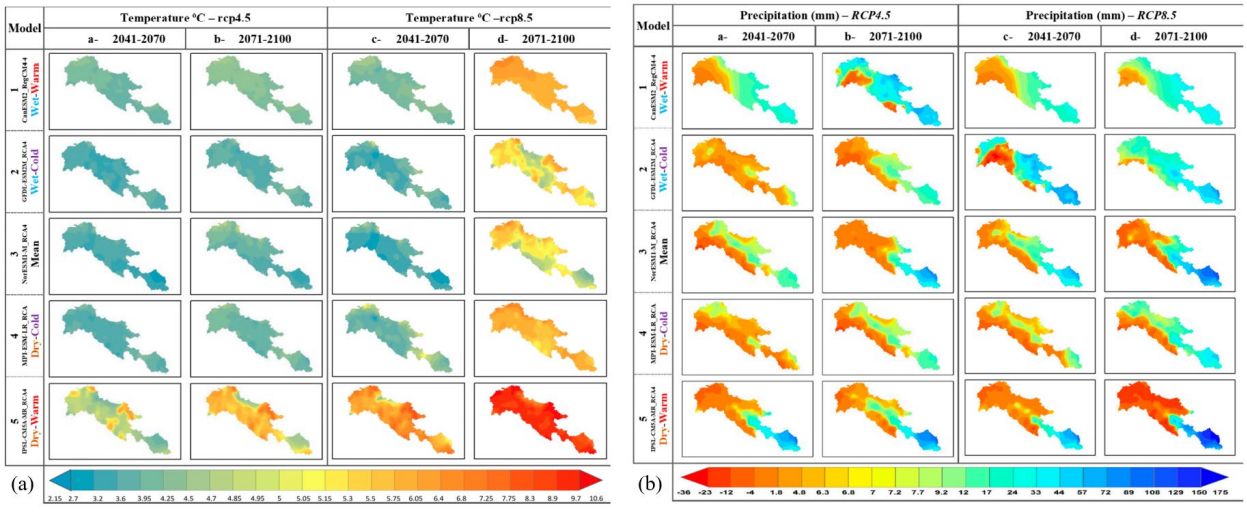

Figure 5: a) Temperature changes and b) precipitation changes in the UIB (Khan & Koch, 2018).

2.3.3.2. Vulnerability to socio-economic changes

Three socio-economic challenges increase the downstream water demand in the Indus Basin (Viviroli et al., 2011). The first challenge is population growth, where the Indus population is expected to increase to 383 million people in 2050 for medium estimates and to 438 million for high estimates (Figure 6; Laghari et al., 2012). Wijngaard et al. (2018) projected population growth based on SSP1 and SSP3, where SSP1/SSP3 represents a low/high growth scenario. The projections are shown in Table 2 and coincide with the projections by Laghari et al. (2012). The growth of big cities is also caused by rapid urbanization, which is the second challenge. By 2050, more than 50% of the Indus population is projected to live in urban areas (Mukherji et al., 2018). United Nations (2018) project that in 2030 40-60% of the Indus population lives in urban areas, compared to 20-40% in 2018. Economic growth is the third challenge, which increases the water demand through a rise in food per capita intake and higher demand for industrial goods (Hussain et al., 2011). Wijngaard et al. (2018) project a rise of 712% in GDP between 2010-2050 for SSP1 and a rise of 359% for SSP3. Between 2050 and 2100, the growth rate decreases to 184% for SSP1 and 148% for SSP3 (Table 2).

When combining the SSP-projections with RCP-projections, the annual water gap is expected to decrease by 21% for RCP4.5-SSP1 in 2100 compared to 1981-2010. For RCP8.5-SSP3, the water gap is expected to increase by 7% for 2100 compared to 1981-2010, mainly due to high population growth (Wijngaard et al., 2018).

Table 2: Population and GDP changes from 2010 until 2100 (Adapted from Wijngaard et al., 2018).

Socio-economic factors and scenario		Years		
		2010	**2050**	**2100**
Population ($x10^6$)	SSP1	245	346	289
	SSP3	245	469	725
GDP (PPP) ($x10^9$ USD 2005)	SSP1	631	5124	14574
	SSP3	631	2894	7191

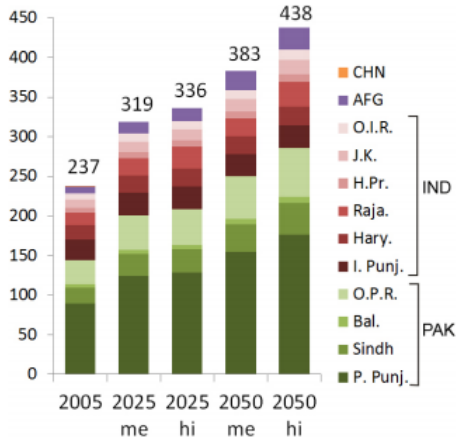

Figure 6: Medium and high population projections in millions for 2025 and 2050 (Laghari et al., 2012).

2.3.3.3. Vulnerability to political and governmental factors

Hydro-political tension entails the risk for political disputes over shared water resources. This tension has been present in Pakistan and India since their independence in 1947, originating from the valuable Kashmir region. To moderate this tension, a conflict resolution mechanism was signed in 1960, known as the Indus Water Treaty (IWT; De Stefano et al., 2017; Qureshi, 2018). In this treaty, the Indus, Jhelum, and Chenab were assigned to Pakistan, whereas Ravi, Beas, and Sutlej were assigned to India. Problems have, however, started to arise due to Indian infrastructure constructions on the upstream rivers assigned to Pakistan (Saqib Riaz et al., 2020; Qureshi, 2018).

According to Farinosi et al. (2018), a combination of exacerbating factors for hydro-political tension are present in the Indus Basin, such as water stress, low government effectiveness and high population density. Therefore, it has the second highest risk for hydro-political tension globally. De Stefano et al. (2017) estimated this risk to be moderate for most parts of the basin, as they included moderating factors.

Weak government effectiveness and institutional resilience play an important role in the hydro-political tension of the Indus Basin (Farinosi et al., 2018). This can largely be attributed to tensions between national, regional, and local institutions. Additionally, water institutions in the basin remain non-participatory (Wescoat Jr et al., 2000).

2.3.3.4. Vulnerability to water stress

Water stress occurs when the total water withdrawals exceed the available amount of water. In the Indus Basin, there is an estimated groundwater depletion rate of 31 to 83 km^3/year (Wijngaard et al., 2018; Qureshi et al., 2010). Figure 7 displays the large spatial variation in groundwater depletion, reaching 1000 mm/year given over the irrigated areas in the Punjab and Haryana provinces, but decreasing towards the west and south (Archer et al., 2010; Cheema et al., 2014; Rasheed, 2013). The aquifer's recharge rate is lowest in the south, thereby increasing the south's vulnerability to water stress (Cheema & Qamar, 2019).

90% of the groundwater exploitation occurs for agricultural use (Rasheed, 2013), causing an unsustainable situation in the long term. In the high-populated areas, about 90% of the people depend on unsustainable groundwater extractions for domestic use (Qureshi et al., 2010).

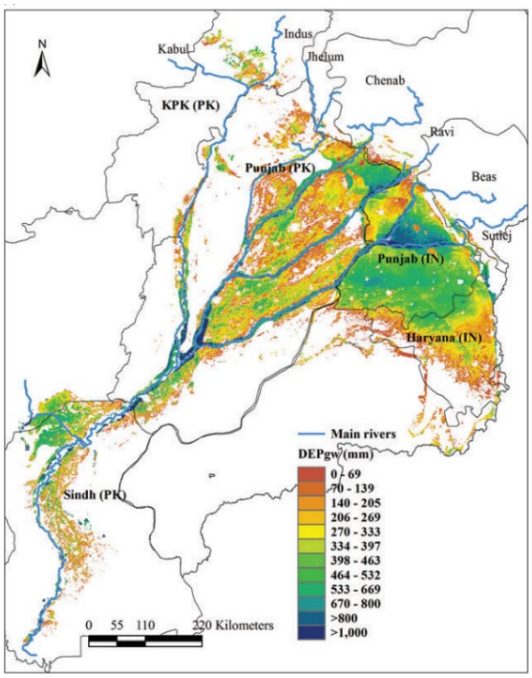

Figure 7: The net groundwater depletion for 1981-2010 (Cheema et al., 2014).

3. Methods

3.1. R and QGIS

R and QGIS are used to do the calculations for this research. The R language and environment is used to model the different steps discussed in section 3.2. Primarily, the raster, sf and gdal packages are used as most data is available in raster and shapefile format (Gimond, 2021). R is additionally used to nicely display the results to the sub-questions. QGIS is an open-source geographical information system, which is mainly used for the subbasin's delineation and checking the outcomes of R (Gimond, 2021).

3.2. Approach

The rWTI and vulnerability scores are derived through several steps by using both global and regional data. These datasets can additionally be found in annex II. The equations to calculate the rWTI are given in annex III and are performed at 0.01˚ resolution, representing the diversity of the area.

Below, the research framework (Figure 8) and analytical framework (Figure 9) are displayed. The research framework displays the general steps undertaken to answer the sub-questions and perform the sensitivity analysis. The analytical framework shows the detailed steps discussed in this section to derive the rWTI and the VI. The boxes on the left/right sight of the indicators represent the steps taken when global/regional data are used.

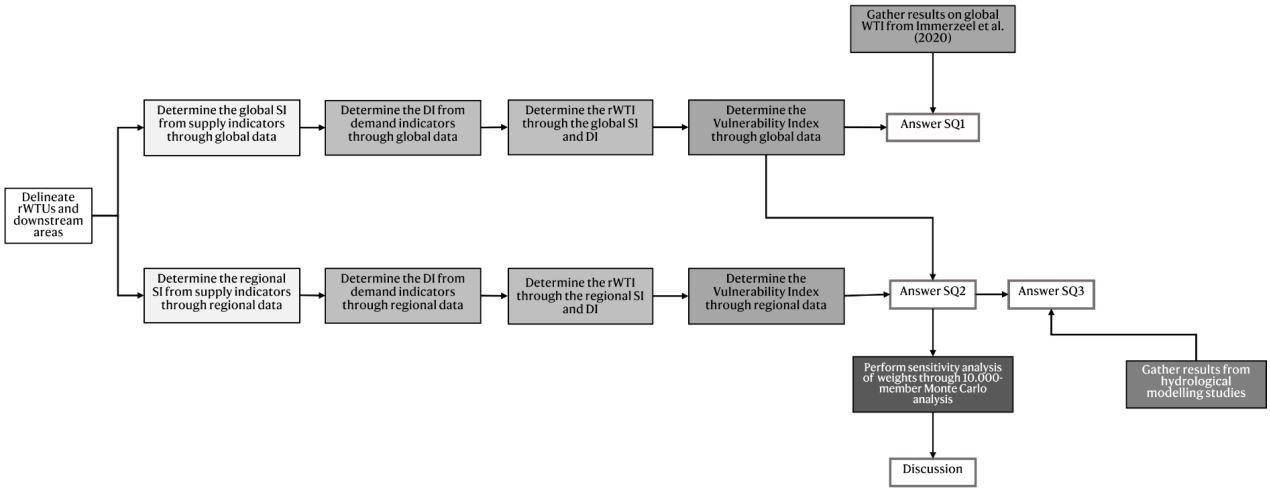

Figure 8: The research framework. The colours correspond to the steps displayed in the analytical framework.

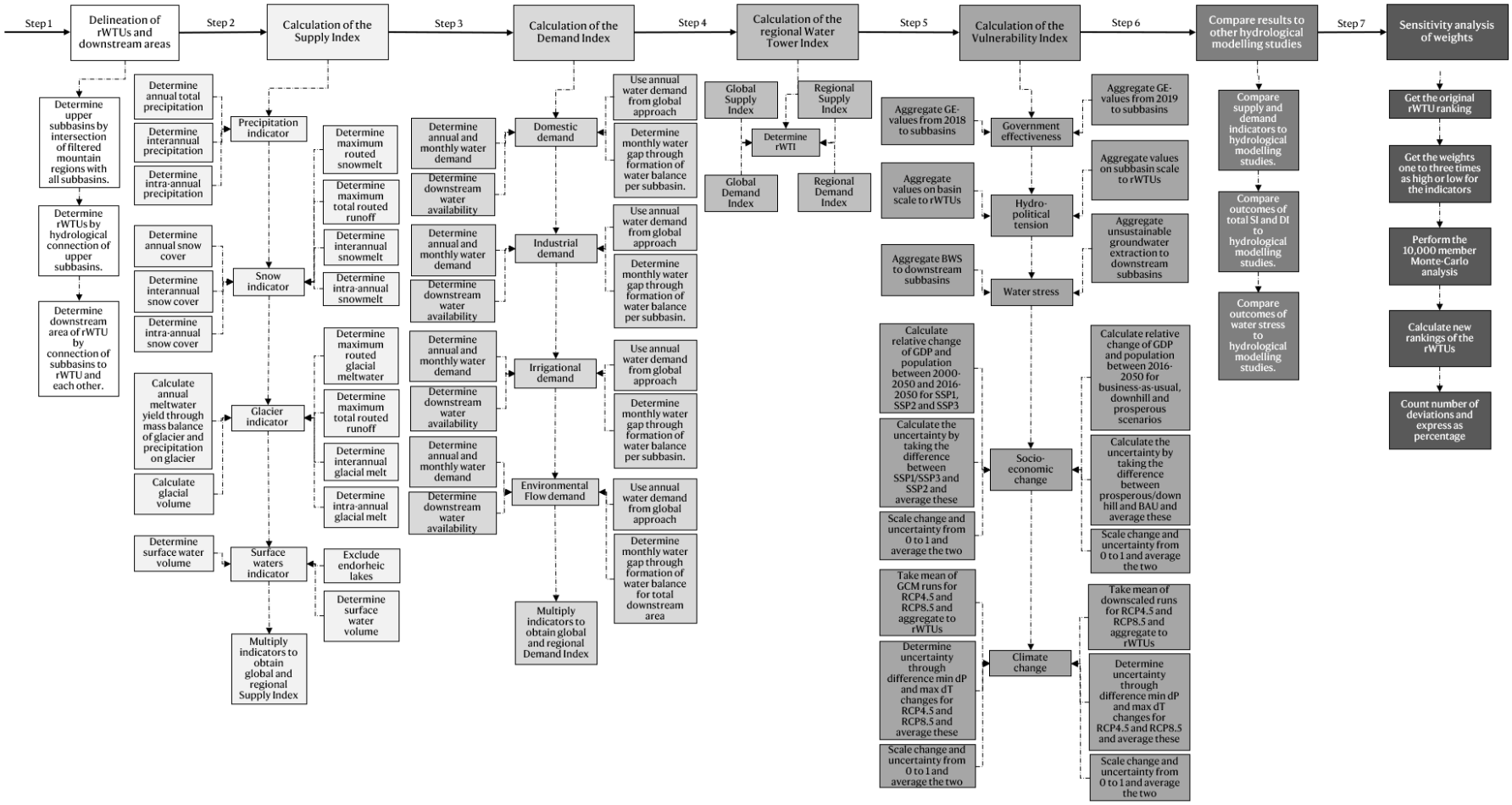

Figure 9: The analytical framework.

3.2.1. Delineation of rWTUs and downstream areas

The Indus Basin consists of different subbasins (Figure 10), derived from Lehner & Grill (2013). This dataset is, together with data from Immerzeel et al. (2020), used to delineate the rWTUs. Data from Immerzeel et al. (2020) contains mountain ranges that have been filtered on criteria (Annex II). This is done to ensure that solely rWTUs with a cryosphere component are included, as the buffering role of the cryosphere is a key characteristic of the water tower (Immerzeel et al., 2020). These mountain ranges intersect with certain Indus subbasins; the upper subbasins. The upper subbasins that are hydrologically connected, indicated in the Lehner & Grill (2013) dataset, form one regional water tower unit (rWTU). Eight rWTUs were determined, shown in Figure 11a. The downstream area of each rWTU is derived through the hydrological connection of the downstream subbasins to the rWTU and to each other. The hydrological connection of the first downstream subbasin to the rWTU is derived from Lehner & Grill (2013). The hydrological connection of the downstream subbasin to other downstream subbasins is derived from Lehner & Grill (2013) and further complemented through data from DIVA-GIS (2011), which displays the hydrological connection between downstream subbasins through smaller waterways. Several rWTUs have similar downstream areas such as rWTUs 3 and 4, however, these downstream areas still have a slightly different downstream area resulting in different outcomes when calculating the indicators. The DIVA-GIS (2011) dataset shows, however, that rWTUs 5 to 8 have the exact same downstream areas as these are highly connected through small waterways. This would result in similar indicator outcomes for these rWTUs. Therefore, for downstream areas 5 to 8, the hydrological connectedness of solely Lehner & Grill (2013) is followed, whereas the high connectedness through the smaller waterways, established through DIVA-GIS (2011), is neglected. The eight rWTUs and their downstream areas are shown in Figure 11b-i. Each rWTU, downstream area and total subbasin is given a new name, based on the major rivers in this subbasin.

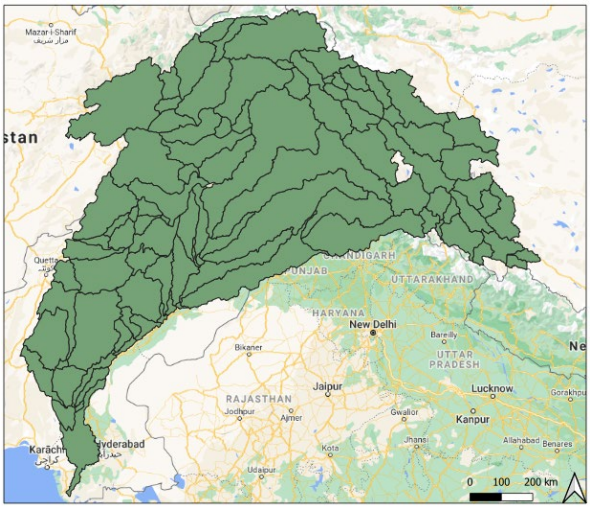

Figure 10: The subbasins within the Indus Basin.

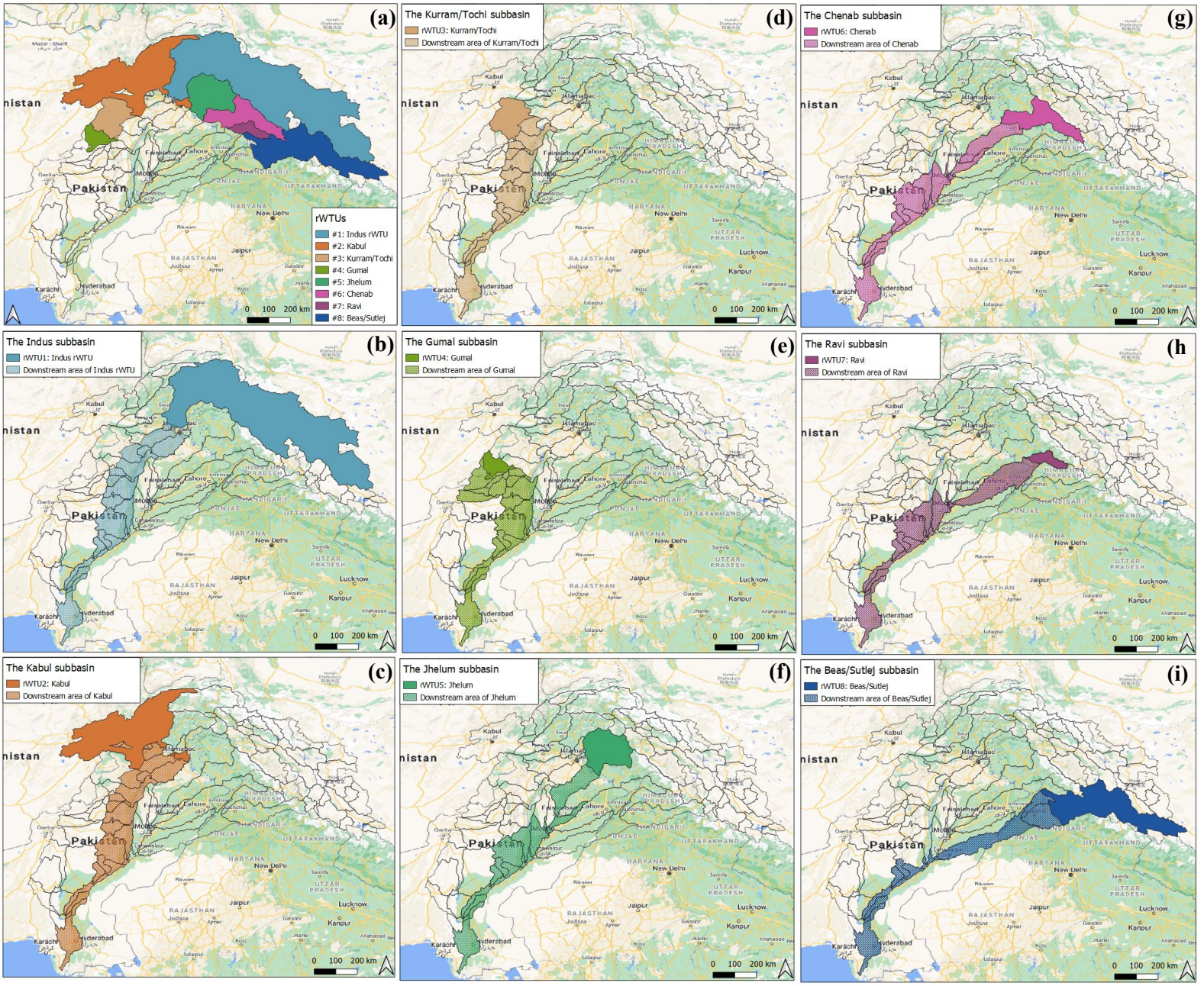

Figure 11: Maps of a) the rWTUs including their number and name and b)-i) the determined subbasins, including their number and name.

3.2.2. Calculation of the Supply Index

For each rWTU, four supply indicators are determined, which are (1)precipitation, (2)snow, (3)glaciers, and (4)surface waters.

To determine the **precipitation indicator (P)** for each rWTU, the average annual total precipitation (P_T), the interannual variability (P_{YV}) and the intra-annual variability (P_{MV}) are calculated using the global ERA5 reanalysis precipitation data ranging from 2001-2017 (Hersbach et al., 2018). Regional precipitation data are available, however there are no regional precipitation datasets coupled to regional evaporation, which are both required to calculate the DI. Regional precipitation data are therefore not used to avoid inconsistencies between the SI and DI outcomes. Precipitation is aggregated to the rWTUs (P_{rWTU}), downstream subbasins, and total subbasin (P_{SUBBAS}), which are then used in the

calculation $P_T=\frac{P_{rWTU}}{P_{SUBBAS}}$. Thereafter, the P_{YV} and P_{MV} are aggregated to the rWTUs, because a rWTU with a consistent water supply scores higher on the SI. The precipitation indicator values are ultimately formed by $P=0.5*(P_{YV}+P_{MV})*P_T$.

The **snow indicator (S)** is determined differently for the global and regional approach. For the global approach, the annual average snow cover from 2001-2017 is derived from MODIS and aggregated to each rWTU, forming the S_T (Hall & Riggs, 2021). This snow cover is used to calculate the interannual variability (S_{YV}) and intra-annual (S_{MV}) variability in snow cover for each rWTU. The global snow indicator is ultimately determined through $S_g=0.5*(S_{YV}+S_{MV})*S_T$. For the regional approach, the snow indicator is determined from the volume of snowmelt and the total basin runoff ranging from 1961-2007, derived from Lutz et al. (2016). For each rWTU, the maximum routed snowmelt (Q_S) and the maximum total routed runoff (Q_{rWTU}) are extracted. Additionally, the interannual variability (S_{YV}) and intra-annual variability (S_{MV}) for each rWTU are determined through monthly runoff, derived from Lutz et al. (2016). The regional snow indicator is ultimately formed by $S_r=(0.5*(S_{YV}+S_{MV}))*(Q_S/Q_{rWTU})$.

The **glacier indicator (G)** is again determined differently for the two approaches. The global approach uses the glacial mass balance (B), derived from the world glacier monitoring service (WGMS, 2020), and uses the glacial area and volume, derived from Farinotti (2019), all ranging from 2001-2017. The precipitation incoming on the glacier (P_{GLAC}) is determined by multiplying the precipitation and the glacial area, which is thereafter aggregated to the rWTUs. The annual meltwater yield (G_Y) for the rWTUs is calculated by $G_Y=(P_{GLAC}-B)/(P_{GLAC}-B+P_{rWTU})$. The glacial ice volume in each rWTU (G_v) is used to calculate the glacial ice storage (G_s) by $G_S=G_V/(G_V+P_{rWTU})$. The global glacier indicator is ultimately formed by $G_g=(G_S+G_Y)/2$. For the regional approach, the glacier indicator is determined from the volume of glacial meltwater and the total basin runoff, ranging from 1961-2007, derived from Lutz et al. (2016). For each rWTU, the maximum routed glacial meltwater (Q_G) and the maximum total routed runoff (Q_{rWTU}) are extracted. Additionally, the interannual variability (G_{YV}) and intra-annual variability (G_{MV}) are determined through monthly runoff. The regional glacier indicator is ultimately formed by $G_r = (0.5*(G_{YV}+G_{MV}))*(Q_G/Q_{rWTU})$.

The **surface water indicator (L)** is first determined through global data, derived from Lehner & Messager (2016), containing 697 lakes for the Indus Basin. The regional approach alters this dataset by removing 47 endorheic lakes where the average long-term discharge flowing through the lake is equal to $0 m^3/s$. The surface water volume (S_L) within each rWTU is extracted. The global surface water indicator is ultimately formed by $L_g=S_L/(S_L+P_{rWTU})$. This is done similarly for the regional surface water indicator, however now by solely using surface water volume from the exorheic lakes ($S_{L,con}$).

The average global SI (SI_g) and regional SI (SI_r) per rWTU are determined by averaging the four global and regional supply indicators. The regional SI differs from the global SI as the glacier and

snow indicators are not taken relative to the total precipitation but taken relative to the total runoff in the rWTU, including snowmelt, glacial melt, and rainfall. Additionally, the regional SI differs from the global SI by excluding endorheic lakes for the surface water indicator.

3.2.3. Calculation of the Demand Index

The DI is based on four indicators: the **domestic demand (D_{DOM})**, the **industrial demand (D_{IND})**, the **irrigation demand (D_{IRR})** and the **EFR (D_{EF})**. For the global approach, the annual and monthly water demand (D_y) for the human indicators is made available by Wada et al. (2016). The natural flow data are made available through Wada et al. (2016), while Gleeson et al. (2012) and Smakhtin et al. (2004) are used to estimate the 90th-percentile exceedance value of the natural flow to obtain the EFR. Annual and monthly evaporation and precipitation data to calculate the downstream water availability are derived from Hersbach et al. (2018). These datasets are adjusted to range from the years 2001 to 2017. For the regional approach, these global datasets are complemented with runoff data from Lutz et al. (2016), ranging from 1961-2007.

For the global approach, first the yearly domestic, industrial and irrigation demand (D_y) are aggregated to the total subbasin. Thereafter, the monthly domestic, industrial and irrigation water demand (D_m) are used. If the D_m for a sector in a grid cell is higher than the monthly water availability (WA_m), given by precipitation minus evaporation, the remaining supply is assumed to come completely from the rWTU. The water gap for a sector is calculated for each cell by D_m - WA_m, which is thereafter aggregated to the downstream subbasin. The monthly water gaps are then summed to yearly water gaps for each sector. The DI-values for the three sectors are ultimately formed by: $\sum(D_m - WA_m)/D_y$.

The regional approach for these three human indicators is similar to the global approach, however, the water gap is calculated differently as it includes the water supply from other rWTUs. Each rWTU contains a downstream area, consisting of different smaller subbasins as was displayed in Figure 11b-i. These smaller subbasins can receive water from multiple rWTUs of which an example is given in Figure 12 where the arrow indicates the first subbasin of each downstream area that overlaps with the downstream area of rWTU1. The water gap of smaller subbasins that are not supplied by other rWTUs (for example subbasin1.1 in Figure 12) is calculated by D_m - WA_m. However, the water gap of smaller subbasins that are supplied by other rWTUs (for example subbasins1.2-1.6 in Figure 12) is calculated iteratively upstream to downstream by D_m - WA_m - Q_{rWTU}. Several smaller subbasins, for example subbasin1.3 (Figure 12), receive a remainder of the water supply from rWTU2 as this supply did not fulfil the demand in the upstream subbasin1.2 ($Q_{rWTU,rem}$; Figure 12). The water gaps for the smaller subbasins are added and the monthly water gaps are summed to yearly water gaps for each human demand indicator. The DI-values for these indicators are ultimately formed by $\sum(D_m - WA_m - Q_{rWTU})/D_y$.

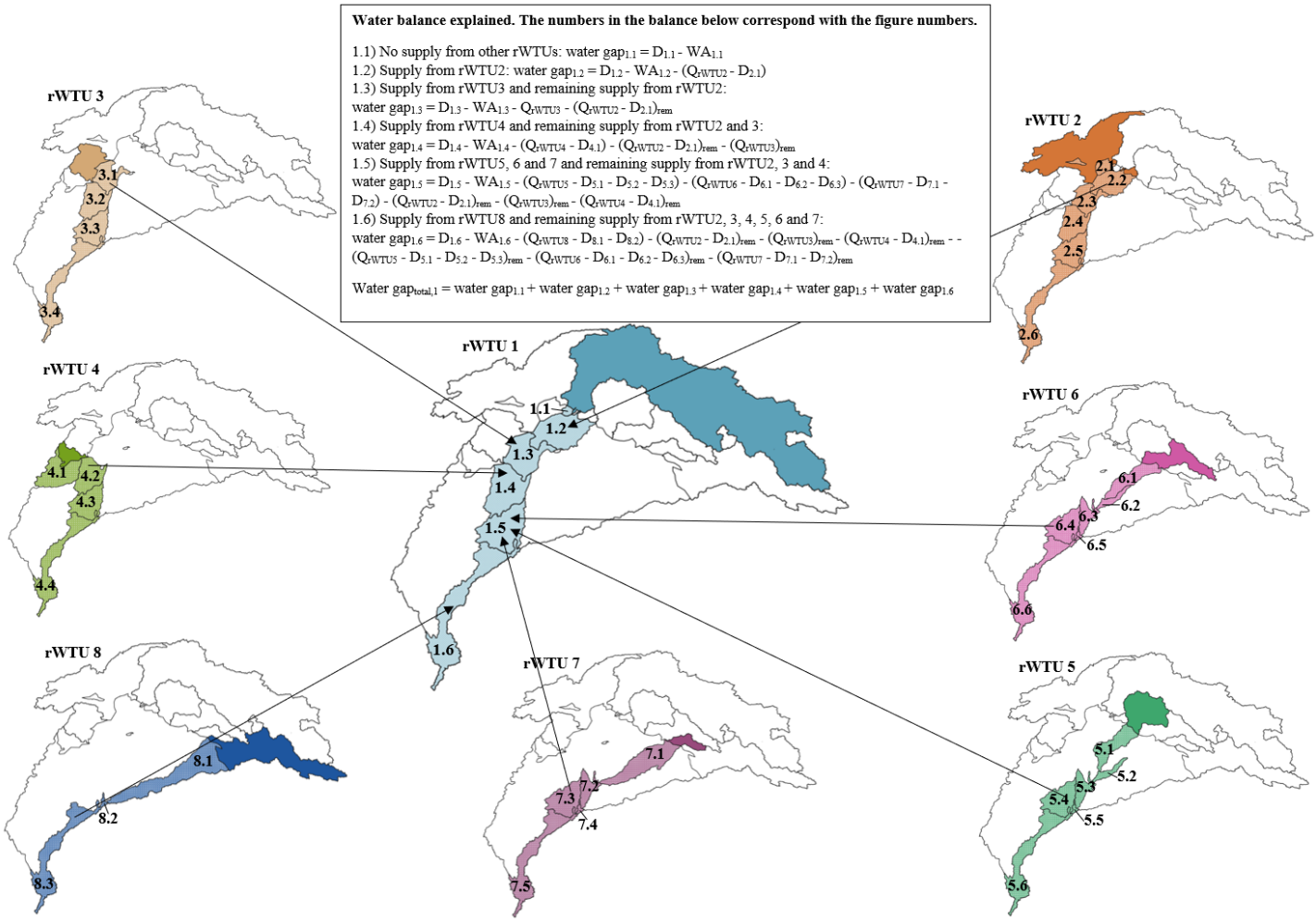

Figure 12: The regional approach to calculate the irrigation, domestic and industrial water gaps of the downstream area of rWTU1. The numbers in the figures indicate the different smaller subbasins within the downstream area and correspond with the subscript numbers in the water balance.

To obtain the global DI-values for the EFR, first the maximum yearly EFR is determined for each downstream area in km^3/year. This maximum EFR value can for all downstream areas be found at the outlet to the Arabian Sea (Figure 13), as the EFR is cumulative. From this maximum EFR, the maximum flows incoming into each downstream area are subtracted (Figure 13). This is done to ensure that solely the yearly EFR within the downstream subbasin is obtained ($D_{EF,y}$). This exact same approach is taken for the monthly EFR data where the two incoming maximum flows are subtracted from the maximum flow at the outlet for each month ($D_{EF,m}$). Additionally, the monthly water availability (WA_m) for the entire downstream area is obtained. The DI-value for the EFR is formed by: $\sum(D_{EF,m} - WA_m)/D_{EF,y}$. The DI_g is ultimately formed by averaging the four global DI-values, one for each sector.

The regional approach for the EFR indicator is similar to the global approach, however, the water gap is calculated differently as it also includes the water supply from other rWTUs in one big water balance for the entire downstream area (Figure 14). It is, however, important to note that not the entire Q_{rWTU} is subtracted from $D_{EF,m}$ - WA_m, but the water supply that is available after the required

EFR for that downstream area is subtracted from it. This is indicated in the water balance in Figure 14 by $D_{max\ out}$ - $D_{max\ in}$, which are determined in the same manner as is indicated in Figure 13. The DI-value for the EFR is formed by $\sum(D_m - WA_m - Q_{rWTU})/D_y$. The DI_r is ultimately formed by averaging the four regional DI-values, one for each sector.

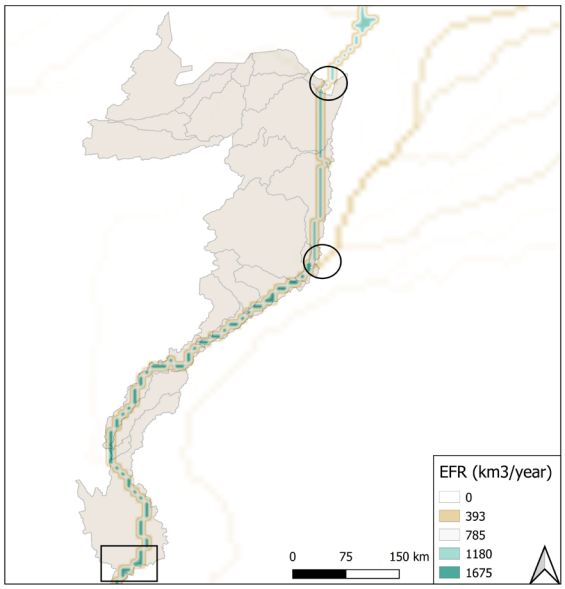

Figure 13: The EFR shown over Gumal. The inflow point [circles] need to be subtracted from the maximum value [square].

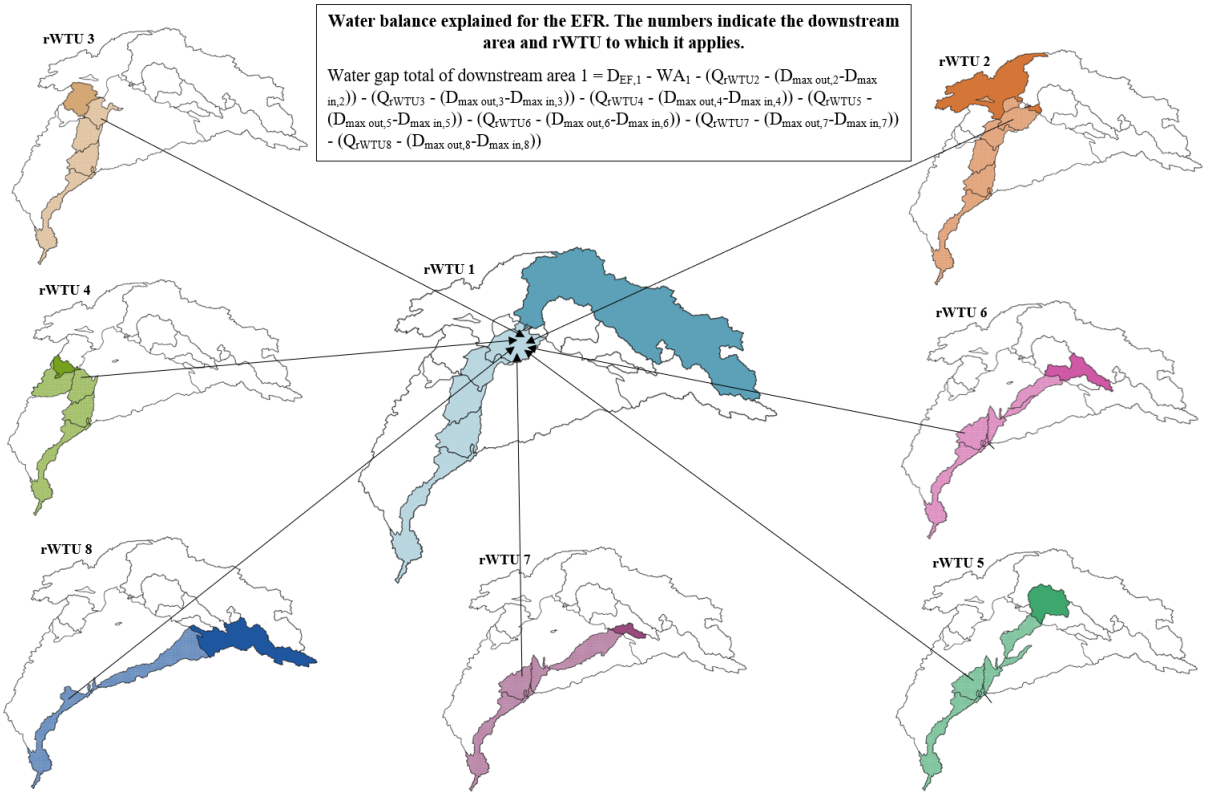

Figure 14: The regional approach to calculate the total EFR water gap of the downstream area of rWTU1. The subscript numbers in the water balance correspond with the numbers of the rWTUs and their downstream areas.

3.2.4. Calculation of the regional Water Tower Index

The rWTI based on global and regional data is calculated by multiplying the global/regional SI by the global/regional DI. The indicators receive an equal weight in their contribution to the SI and DI. Afterwards, the rWTI values are normalized to the maximum value found.

3.2.5. Calculation of the Vulnerability Index

Vulnerabilities of the water supplying role of the rWTUs are assessed, consisting of three static indicators and four dynamic indicators. The static indicators are **governmental effectiveness**, **water stress** and **hydro-political tension**. The indicators of change consist of **climate changes**, which are precipitation changes (dP) and temperature changes (dT), and **socio-economic changes**, which are population changes and GDP changes.

GE is used as a proxy for water management capacity. Because it is given per country, no difference in global and regional data can be made, however, for the regional approach the most recent data from 2019 are used. The data are derived from Kaufmann & Kraay (2019). Values range from -2.5 to +2.5, where -2.5 indicates the highest vulnerability and + 2.5 the lowest vulnerability. The GE values are aggregated to the different subbasins (total of rWTU and downstream areas), as several subbasins overlie multiple countries, and the area-averaged value is calculated.

For hydro-political tension, both global and regional data are derived from UNEP-DHI & UNEP (2016). A risk level of 1 represents low risk for hydro-political tension, while 5 indicates the highest risk. The hydro-political tension is aggregated to each rWTU, as this gives a larger diversity than aggregation to the total subbasins due to overlap of the downstream areas. Each rWTU receives an integer value based on the modal value for both the global and regional approach.

BWS and unsustainable groundwater extraction function as indicators for water stress. The BWS values for 2014, derived from Hofste et al. (2019), are used for the global approach. The area averaged BWS is aggregated to the downstream subbasins, where 5 indicates most competition among users and 0 indicates fairly to no competition. For the regional approach, an estimate of the annual unsustainable groundwater extraction, derived from Biemans et al. (2019), is used, and its sum is aggregated to the downstream subbasins. The outcomes of both unsustainable groundwater extraction and BWS are scaled from 0 to 1 for comparison, where 1 indicates the highest vulnerability and 0 the lowest vulnerability to water stress.

For the dynamic indicators, first changes in GDP (dGDP) and population (dPop) are calculated for the entire subbasin, which are based on the three shared-socio-economic pathways (SSPs). Global data on both GDP and population changes are derived from Murakami & Yamagata (2019) for the years 2000 and 2050 to ensure a comparison can be made to the outcomes of Immerzeel et al. (2020). The year 2000 in SSP2 is used as the reference year, whereas for the year 2050 SSP1, SSP2 and SSP3

scenarios are analysed. SSP2 functions as the mean of the projections, whereas SSP1 and SSP3 represent the extremes and thereby the uncertainty. First the mean values for dPop and dGDP in SSP2 from 2000-2050 are scaled from 0 (no change) to 1 (highest change). Second, the difference between the changes of SSP2 and SSP3 are taken, as well as the changes between SSP2 and SSP1. Both these differences are scaled between 0 (no uncertainty) and 1 (highest uncertainty in dPop and dGDP) and the average of this is taken. This is repeated with 2016 as reference year, as this is the reference year in the regional dataset. Regional data is gathered from Smolenaars et al. (under review), where downscaled population and GDP data are available for 2016 and where business-as-usual, downhill, and prosperous projections for both population and GDP are available for 2050. The changes from 2016 to 2050 for business-as-usual function as the mean of the projections, whereas the downhill and prosperous changes in 2050 compared to 2016 represent the uncertainty. The same approach is taken, however now for these regional scenarios. The average of the dPop/dGDP and the uncertainty forms the vulnerability to population and GDP changes.

Lastly, changes in the climate indicators, dP (%) and dT (˚C), are determined for the rWTUs. For the global dataset, changes from 2036-2065 compared to 1986-2001 are made available by A. Lutz, whereas for the regional dataset changes from 2071-2100 compared to 1971–2000 are derived from Lutz et al. (2016). 35 GCM runs for RCP4.5 and 32 GCM runs for RCP8.5 are used to obtain the mean change per rWTU for the global approach (Table 3), whereas four GCMS are used for the regional approach (Table 4). The mean dP and dT of the RCP4.5 and RCP8.5 runs are calculated, as well as the maximum decrease in precipitation and maximum increase in temperature. These are used to calculate the climate uncertainty within each rWTU. The larger the decrease in precipitation and increase in temperature to the mean, the higher the rWTU's uncertainty. First, the mean values for both dP and dT for the individual rWTUs are scaled from 0 to 1. For temperature, 0 indicates no change in temperature, whereas 1 indicates the highest change in temperature. For precipitation, no change or an increase in precipitation is deemed 0, whereas 1 indicates the highest decrease in precipitation. Second, the uncertainty for each rWTU is scaled between 0 (no uncertainty) and 1 (highest uncertainty). The average of the dP/dT and climate uncertainty forms the vulnerability to precipitation and temperature changes of the rWTU.

Table 3: The included GCM runs for the global approach (Lutz et al., 2016).

RCP	GCM	
RCP4.5 and RCP8.5	ACCESS1.0	GISS-E2-R
	ACCESS1.3	HadGEM2-A
	BCC-CSM1.1	HadGEM2-CC
	BNU-ESM	HadGEM2-ES
	CanESM2	INMCM4.0
	CCSM4	IPLS-CM5A-LR
	CESM1(BGC)	IPLS-CM5A-MR
	CESM1(CAM5)	IPLS-CM5B-LR
	CMCC-CMS	MIROC-ESM-CHEM
	CMCC-CM	MIROC-ESM
	CNRM-CM5	MIROC5
	CSIRO-Mk3.6.0.	MPI-ESM-LR
	EC-EARTH	MPI-ESM-MR
	FGOALS-g2	MRI-CGCM3
	FIO-ESM	NorESM1-M
	GISS-E2-H	NorESM1-ME
Solely RCP4.5	BCC-CSM1.1m	
	GISS-E2-H-CC	
	GISS-E2-R-CC	

Table 4: The included GCM runs for the regional approach.

RCP	Scenario	GCM
RCP4.5	DRY, COLD	Inmcm4_r1i1p1
	DRY, WARM	IPSL-CM5A-LR_r3i1p1
	WET, COLD	MRI-CGCM3_r1i1p1
	WET, WARM	CanESM2_r4i1p1
RCP8.5	DRY, COLD	MPI-ESM-LR_r1i1p1
	DRY, WARM	IPSL-CM5A-LR_r3i1p1
	WET, COLD	CSIRO-Mk3-6-0_r1i1p1
	WET, WARM	MIROC5_r3i1p1

3.2.6. Sensitivity analysis of weights

To calculate the rWTI, each indicator was assigned a weight of 1, meaning each indicator contributes equally to the rWTI. There is, however, uncertainty present in the weight of each indicator, because one indicator, for example snow, could in practice be more important in determining the rWTI than another indicator, for example precipitation. Hence, a sensitivity analysis is performed in which the weights of each of the supply and demand indicators is varied randomly. Thereafter, I show how this affects the ranking of the rWTUs in the rWTI calculation. The weight of each indicator is assumed to be normally distributed, can be between one and three times as high or low as the weight of another indicator and is assessed through a 10,000-member Monte Carlo analysis.

4. Results and discussion

4.1. Increased spatial resolution of the WTI for better representation of spatial variability

To determine whether application of the global WTI at subbasin scale provides better representation of spatial variability, thereby answering sub-question 1, global datasets are used on subbasin scale. The outcomes are compared the outcomes derived by Immerzeel et al. (2020), who used global datasets on basin scale.

The rWTUs display large variability in the supply indicator outcomes (Figure 15), especially for the glacier (sub-)indicators, where the indicators are as low as 0 for Gumal and Kurram/Tochi and are up to 0.9-1 for the remaining rWTUs. The glacier water yield is low for the Indus WTU compared to the rWTUs, likely due to using the total Indus mass balance instead of small mass balances for the separate rWTUs. Large variability is also present in the snow (sub-)indicator outcomes. The interannual variability seems to be overestimated in the global WTI-approach, likely due to the different maximum and minimum values found for the Indus WTU and rWTUs. The higher scoring rWTUs on interannual and intra-annual variability also score higher on the total snow indicator. This is likely due to the snow-albedo feedback, as areas with low interannual and intra-annual variability are more consistently covered with snow. This thereby keeps the albedo high, ensuring a higher reflection of sunlight, which will sustain the snow-covered area. The WTU outcome for the snow and glacier indicators does provide somewhat of an average value compared to the rWTU outcomes. The total Indus WTU scale does, however, not capture the large spatial variability between the rWTUs, which does indicate the need for a more regional approach. For the precipitation indicator, the Indus WTU is high compared to the rWTUs, likely due to the differing interannual and intra-annual variability caused by differing maximum and minimum values within each rWTU and the WTU. The influence of the westerlies on Kabul and the Indus rWTU, and the orographic precipitation in the Indus rWTU, Kabul and Jhelum become evident from the results. Additionally, the high mountain ranges in these rWTUs ensure a lower intra-annual variability. The lake indicator displays large varieties in the volume of lakes where Beas/Sutlej, Ravi, and the Indus rWTU score highest. Kabul and Jhelum also contain a high number of lakes, however, these rWTUs score low for the lake indicator, likely because these lakes are largely formed by precipitation input. The Indus WTU again takes on an average value for the lake indicator, thereby not accounting for the regional differences in lake volume and precipitation input.

From Figure 16, displaying the demand indicators, it becomes evident that the subbasins score higher on the irrigation, domestic and industrial demand indicators compared to the total Indus Basin. This is likely because the water availability ends up being lower when calculated on subbasin scale compared to basin scale, resulting in a higher water gap and therefore a higher demand indicator. The EFR indicator of the Indus Basin is, however, much higher (0.84) compared to the subbasins (0.049-

0.0125). The smaller EFR-values for the subbasins are likely caused by solely subtracting the main flows from the outflow, while small waterways flowing into the downstream area are not subtracted. This could result in a smaller yearly EFR and consequently produce a larger DI-value.

Figure 17, displaying the total SI, DI, (r)WTI, and normalized (r)WTI, first shows a slight overestimation of the DI-value for the Indus Basin compared to the rWTUs, likely caused by its much higher EFR-value. There is variability in the DI-values of the rWTUs, however, this is small compared to the variability in the SI-values. The total Indus WTU seems to take on the average value, thereby neglecting the large variety amongst the rWTUs. For the (r)WTI-values, the Indus WTU solely deviates largely from Gumal and Kurram/Tochi. The rWTI outcomes still display variabilities, compared to which the WTI outcome is high, likely caused by the higher snow and glacier indicators, and DI-value found by Immerzeel et al. (2020).

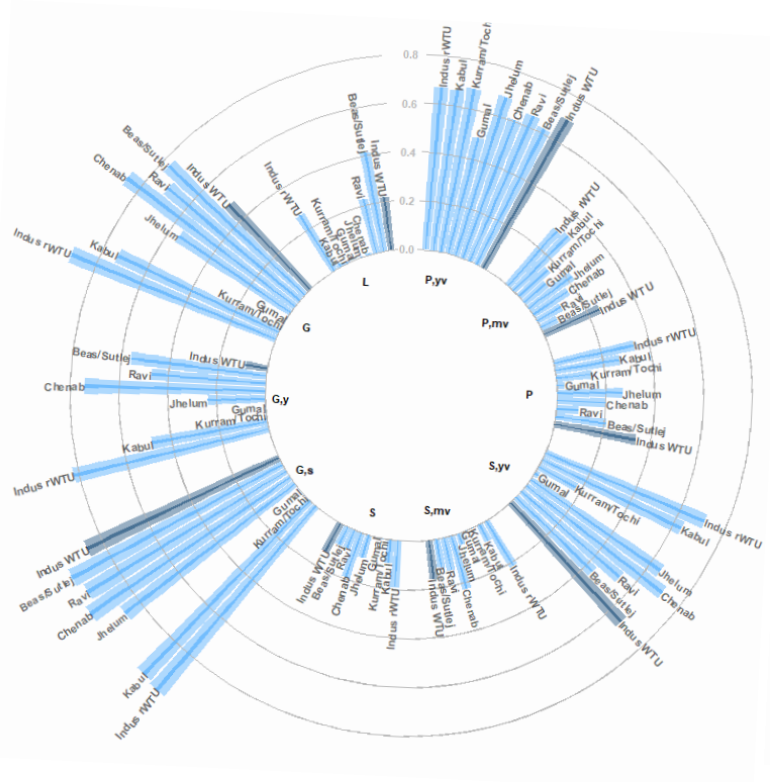

Figure 15: Supply indicators for the Indus WTU (dark colour) and Indus rWTUs (lighter colours).

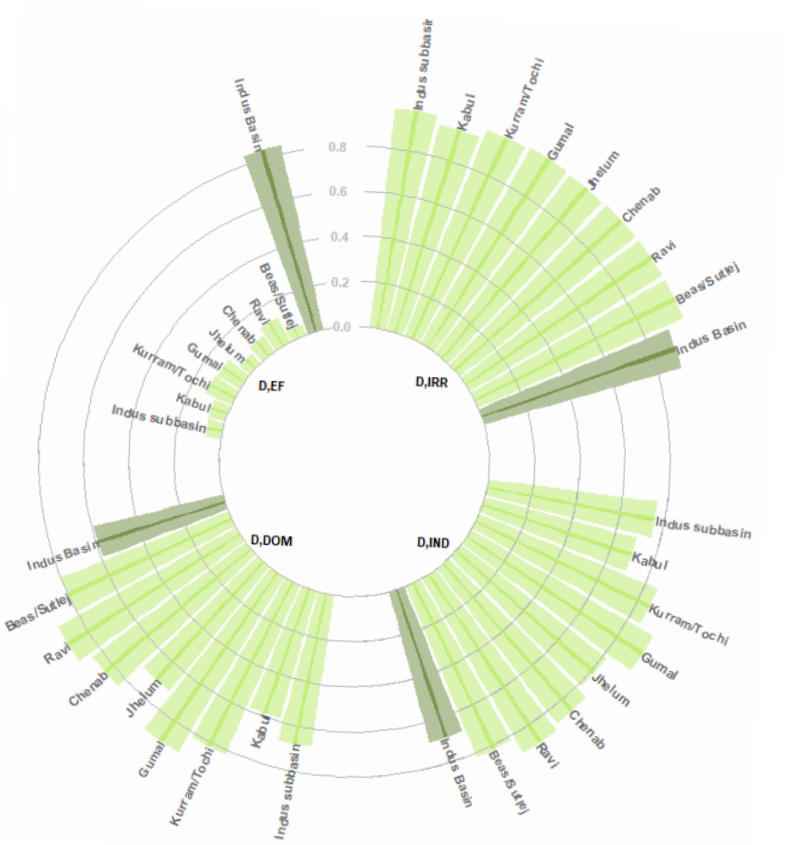

Figure 16: Demand indicators for the Indus Basin (dark colour) and Indus subbasins (lighter colours).

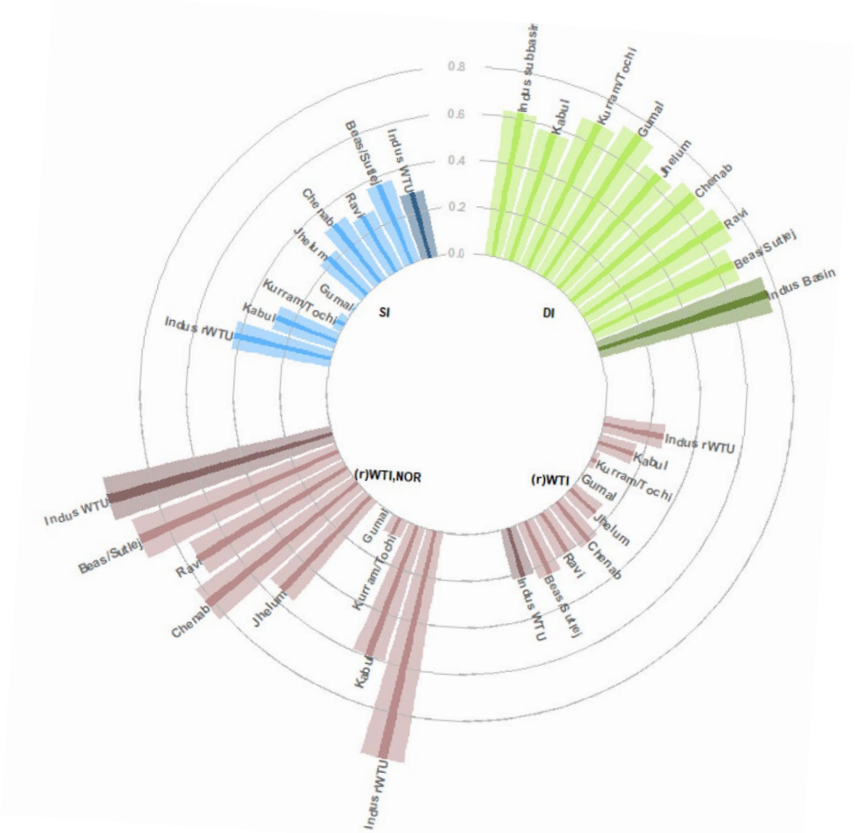

Figure 17: SI, DI and (r)WTI of the Indus Basin/WTU (darker colour) and Indus subbasins/rWTUs (lighter colours).

Figure 18, displaying the VI-outcomes, shows large varieties in the indicator values of the subbasins/rWTUs, when compared to the total Indus Basin/WTU. For the BWS, displayed in Figure 18c, the total Indus Basin takes on the average value of the subbasins, where the eastern subbasins score much higher on water stress. The Indus Basin also takes on the average value of the subbasins for GE, displayed in Figure 18a, however again the large variability in outcomes between the subbasins is not considered. The hydro-political tension, displayed in Figure 18b, does, on the other hand, not show any variability as the global dataset does not consider regional variability.

For both the socio-economic and climate change indicators, presented in Figure 18d-g, the outcomes of the total Indus Basin/WTU seem to be underestimated compared to the outcomes of the Indus subbasins/rWTUs, especially for population change and temperature change. This underestimation could be due to different derived means for the Indus WTU/Basin compared to the rWTUs/subbasins. Large variabilities between the subbasins/rWTUs are especially present for population change and precipitation change, where west and centrally located subbasins/rWTUs experience the highest vulnerability. This is mainly caused by the mean change instead of the uncertainty. This high uncertainty on changes in the subbasins/rWTUs is evident for all socio-economic and climate indicators, thereby clarifying the importance that these are taken into consideration when determining their indicator value.

The application of the WTI and VI at subbasins scale provides a better representation of spatial variability as most indicators display large variabilities within the Indus Basin/WTU. The values for the total Indus WTU do provide an average value of the rWTUs for several indicators, but this still underestimates the large regional variability. The exact values behind all the figures and the unscaled values for the dynamic vulnerability indicators can be found in annex IV.

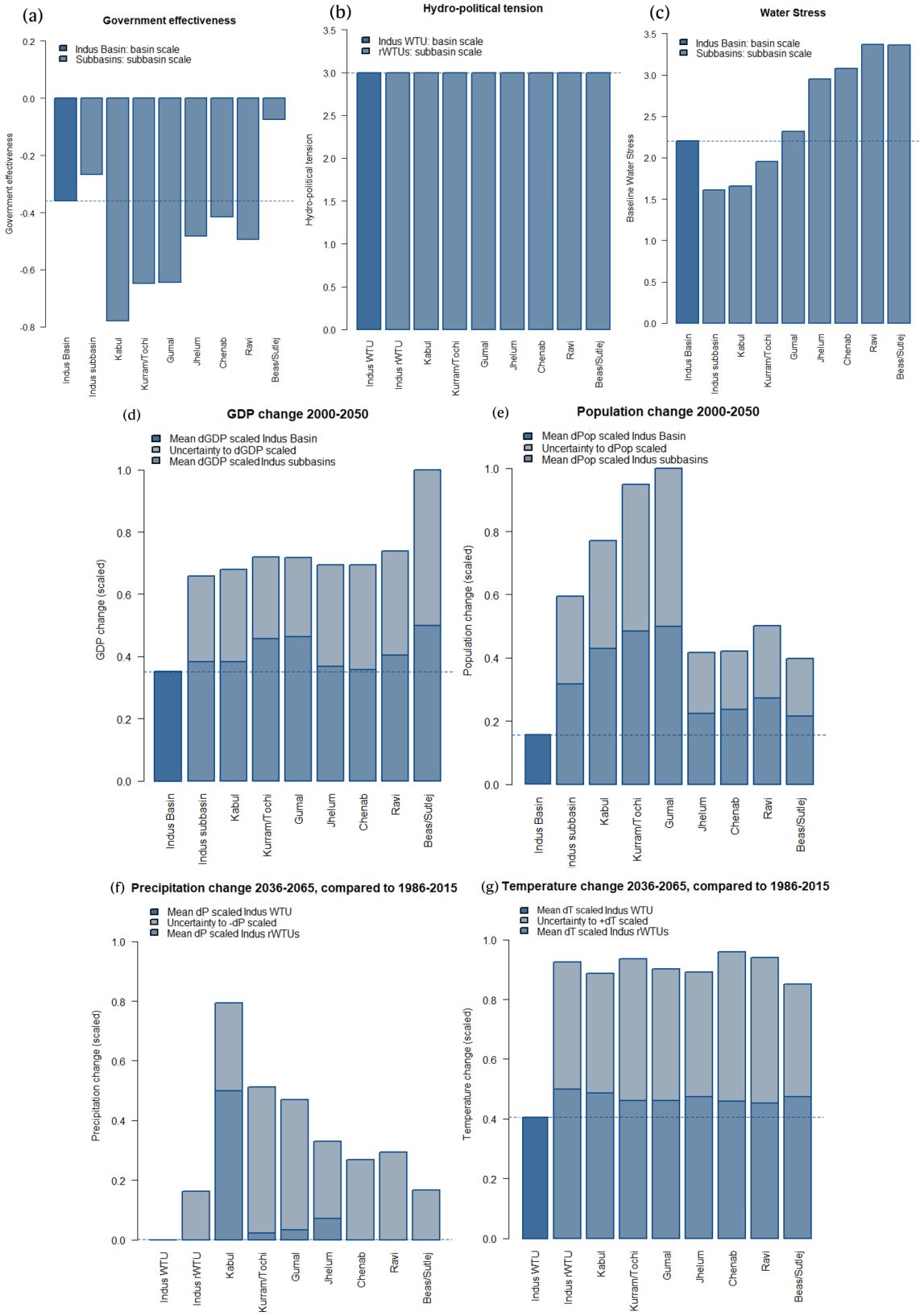

Figure 18: VI of the Indus Basin/WTU (dark colour) and Indus subbasins/rWTUs (lighter colours).

4.2. Use of regional data

To determine whether the use of regional data over global data changes the outcomes, thereby answering sub-question 2, regional datasets were used on subbasin scale. The outcomes obtained are compared to the outcomes derived using global data on subbasin scale (Section4.1).

Figure 19 displays the supply indicator outcomes, excluding precipitation as this has not been altered through regional data (Section3.2.2.). The lake indicator has solely changed for the Indus rWTU, as this was the only rWTU including endorheic lakes. For the snow and glacier indicators, however, large changes have occurred when using regional data over global data as this changes the calculation approach. First, the snow (sub-)indicators have decreased largely in value, and their ranking has changed. Chenab, the highest scoring rWTU when global data is used, has changed to Kabul when using regional data. Furthermore, Jhelum has decreased largely in value, whereas the Indus rWTU, Kabul and Beas/Sutlej remain important. The higher scoring rWTUs on low interannual and intra-annual variability again score high on the total snow indicator, likely due to the snow-albedo feedback. The use of regional data over global data has caused all glacier indicators to decrease significantly, while the ranking among the rWTUs remains similar. An important change, however, is that the Indus rWTU scores highest when using global data, whereas this is Chenab when using regional data.

Figure 20, displaying the demand indicators, shows a decrease in all the demand indicator values when using regional data over global data. By taking the water supply from other rWTUs into account, the water gap becomes smaller, leading to both smaller indicators and a different ranking of the subbasins. The EFR indicator changes to zero for all subbasins, as the discharge from other rWTUs closes the water gap of the EFR.

In Figure 21, the overall results of the rWTI are displayed. The SI-values have decreased for all rWTUs when using regional data over global data, except for Gumal, while the ranking of the rWTUs has not changed. The DI-values decreased largely due to the inclusion of the water supply from other rWTUs in the water balance. The ranking among the subbasins also changed, caused by the large water supplies of the Indus rWTU, Jhelum and Kabul. These rWTUs hereby close the water gap for the other subbasins. The eastern subbasins score highest on the DI, indicating a higher population and lower water supply. The importance and ranking of the rWTUs in the (normalized) rWTI also changed; when using global data, the Indus rWTU scores highest, whereas this is Beas/Sutlej when using regional data. The top four rWTUs change in position when using regional data over global data, however the four lowest do not. This displays large differences when using regional data compared to global data.

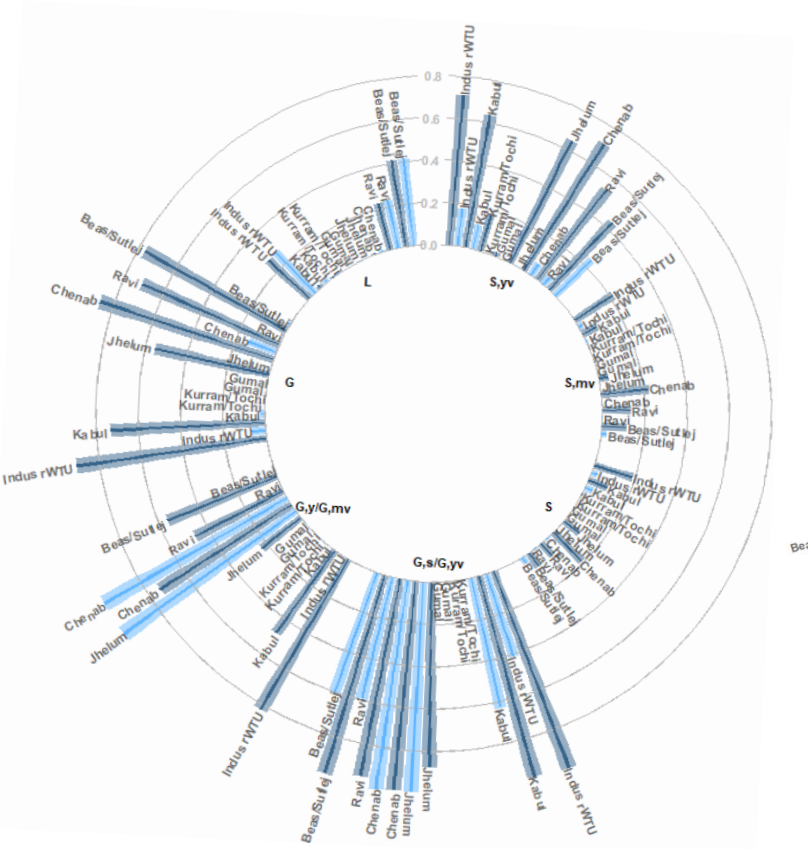

Figure 19: Supply indicators of Indus rWTUs using global data (dark colour) and regional data (lighter colours).

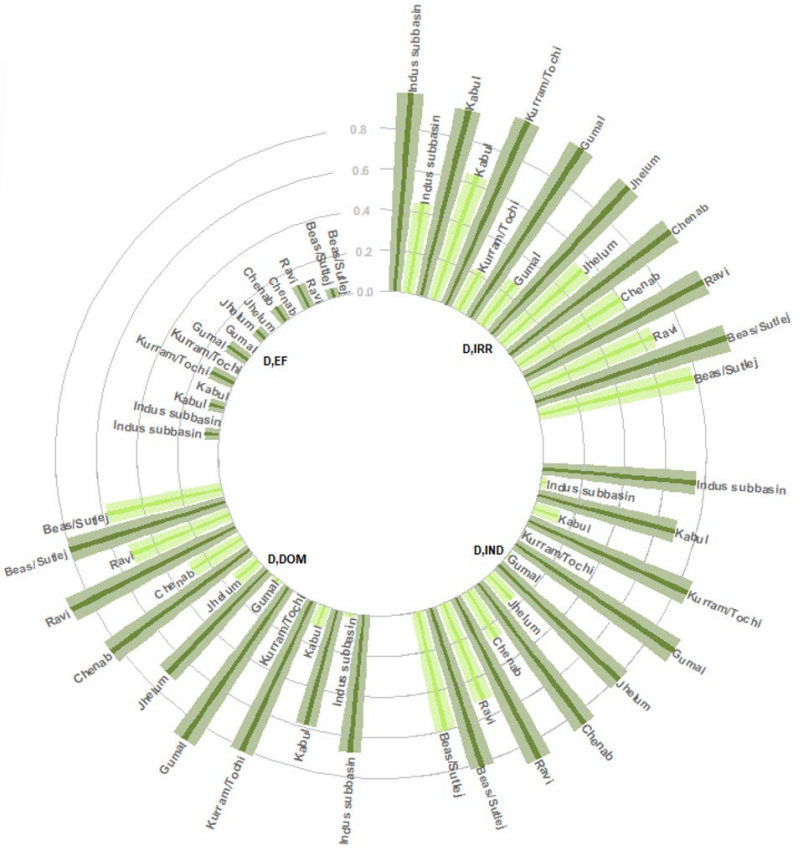

Figure 20: Demand indicators of Indus subbasins using global data (dark colour) and regional data (lighter colours).

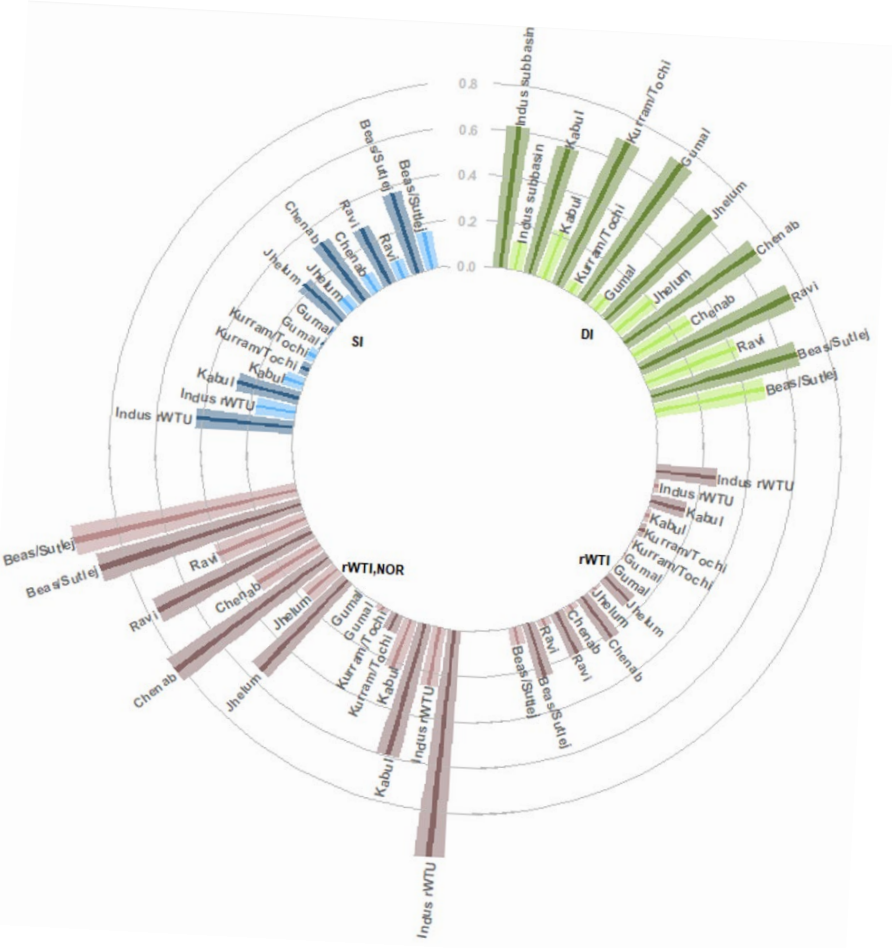

Figure 21: SI, DI and rWTI of the Indus subbasins/rWTUs using global data (darker colour) and regional data (lighter colours).

Figure 22a, displaying GE, shows that the use of more recent data does decrease the vulnerability of the subbasins slightly, but the vulnerability remains high due to the lacking coordination between national, regional, and local institutions (Westcoat Jr et al., 2000). Beas/Sutlej has the highest GE, likely because it lies in India instead of Pakistan. Figure 22b, displaying hydro-political tension, indicates that the use of regional data leads to a larger variability in the vulnerability of the rWTUs. The hydro-political tension changes for 5 out of the 8 rWTUs, ranging from 2 to 5. The Indus rWTU, Chenab and Ravi experience the highest hydro-political tension. This coincides with De Stefano et al. (2017) who discovered higher hydro-political tensions in the centre UIB due to the large infrastructure constructions. Figure 22c, displaying water stress, shows there are large differences when using global data over regional data. When the BWS is used as global indicator, the values are especially high in the eastern downstream areas, which changes to the northeast and west when unsustainable groundwater extraction is used as regional indicator. This is likely because the unsustainable groundwater extraction differs from the BWS indicator in two ways. First, the unsustainable groundwater extraction dataset solely considers groundwater withdrawals for agriculture. The domestic demand, which the BWS does consider, is however largely fulfilled with unsustainable groundwater extractions (Archer et al., 2010; Wijngaard et al., 2018). Domestic withdrawals are highest in the eastern basins, therefore explaining why the BWS is particularly high here. Second, the unsustainable groundwater extraction dataset solely considers groundwater withdrawals, while the BWS also considers surface water extractions. These surface water extractions are, however, particularly large for agriculture, which coincides with the eastern downstream areas (Wijngaard et al., 2018).

The socio-economic indicators, displayed in Figure 22d and 22e, indicate that the GDP change remains similar for most subbasins, while decreasing for Kurram/Tochi and Gumal. This decrease is due to the smaller GDP change in Afghanistan, where these subbasins lie. Population changes increase when using regional data over global data for all subbasins, except Kurram/Tochi and Gumal. This can likely again be attributed to their location in Afghanistan, which the regional data considers more.

The temperature indicator (Figure 22g) remains similar for all rWTUs when using regional data over global data, while showing little diversity between the rWTUs. The ranking of the rWTUs does change; the highest-ranking rWTU changes from Chenab to the Indus subbasin. The vulnerability to precipitation change varies largely amongst the rWTUs. Figure 22f shows that the same rWTUs display a decreased precipitation for both global data and regional data. The amount of change, however, differs largely between the two datatypes. The uncertainty is higher when using regional data, which could be due to using the four most extreme GCMs to make the projections with (Table 4).

The use of regional data over global data changes the rWTI and VI for all indicators to a different extent in both value and ranking. Large changes especially occur for the DI, water stress and vulnerability to precipitation. The exact values behind the figures can be found in annex V, as well as the unscaled values for the dynamic vulnerability indicators and water stress.

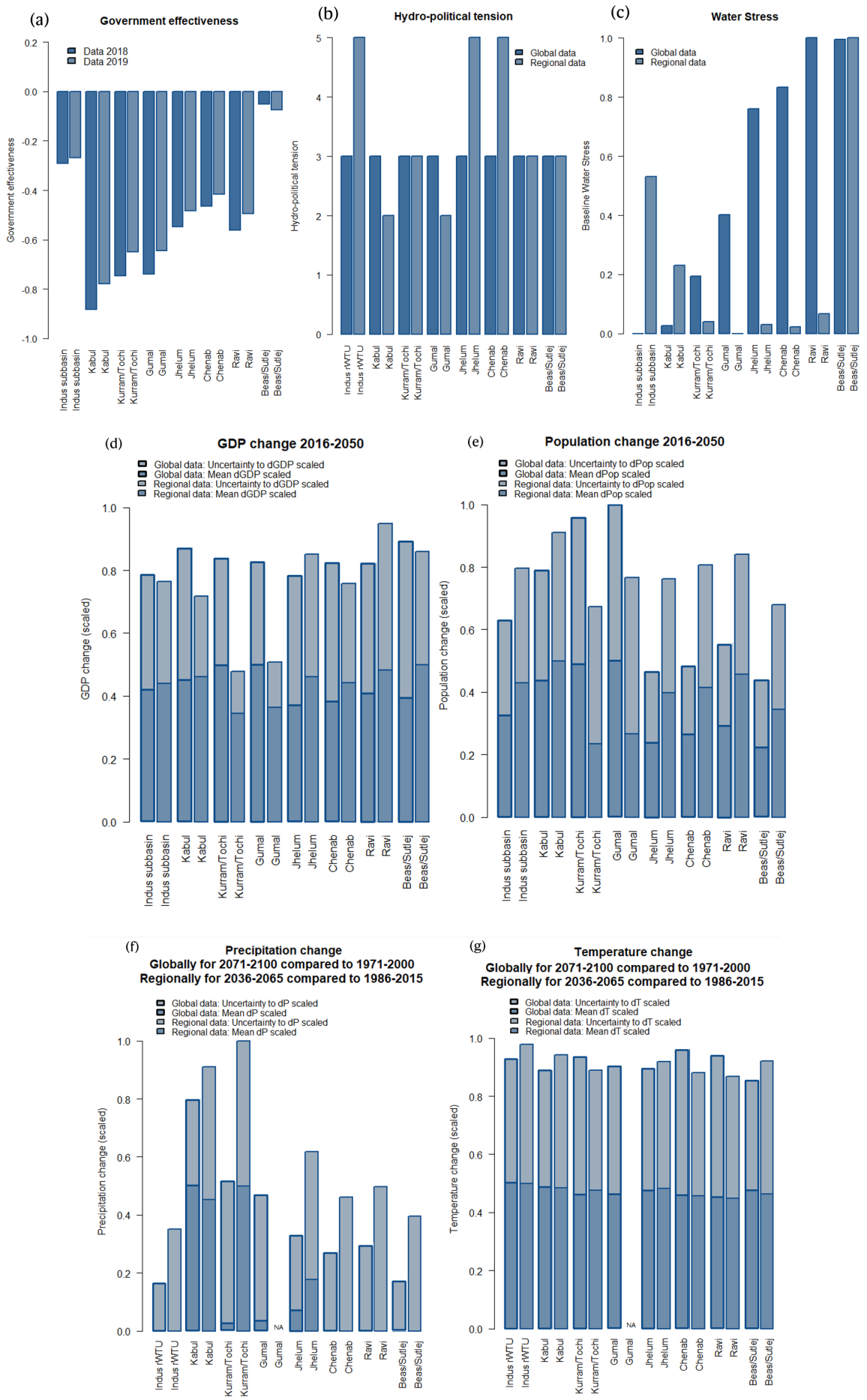

Figure 22: VI of Indus subbasins/rWTUs for global/older data (dark colour) and regional/recent data (lighter colours).

4.3. Comparison to subbasin scale hydrological studies

To determine whether the conclusions drawn through the rWTI coincide with conclusions drawn in hydrological models at subbasin scale, thereby answering sub-question 3, a comparison is made between the outcomes derived through regional data (Section4.2) and hydrological studies.

Studying the supply indicators first clarifies that the Indus rWTU scores highest on the precipitation indicator, followed by Jhelum and Kabul (Figure 15). Immerzeel et al. (2015) and Immerzeel et al. (2009) clarified that the highest precipitation amounts are found on the arc of the southern Himalaya due to the westerlies, while the lowest precipitation amounts are found in the northeast and southwest of the UIB. The hotspot for high precipitation in the northeast coincides with the locations of the Indus rWTU, Kabul and Jhelum (Figure 23a and 23b). The Indus rWTU and Kabul do contain large dry areas, however, the intra-annual variability of the Indus rWTU is smallest (Figure 24), which still explains why it is one of the hotspots. For several rWTUs information is missing, therefore their intra-annual variability cannot be determined. Figure 15 also displays that the lowest scoring rWTU are Gumal, Ravi and Kurram/Tochi, which can mostly be attributed to the lower amount of precipitation and higher intra-annual variability in these rWTUs. This coincides with Figure 23a and 23b, where these southern located rWTUs receive less rainfall, as the climate becomes dryer. For precipitation, the results therefore coincide well with the conclusions drawn from the rWTI-approach.

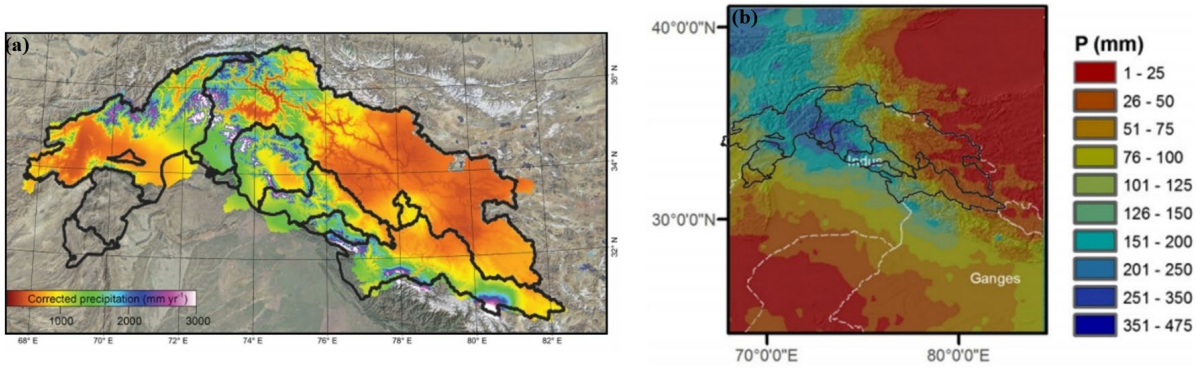

Figure 23: a) Precipitation over the UIB overlain by an outline of the rWTUs (Adapted from Immerzeel et al., 2015). b) Precipitation over the UIB overlain by an outline of the rWTUs (Adapted from Immerzeel et al., 2009).

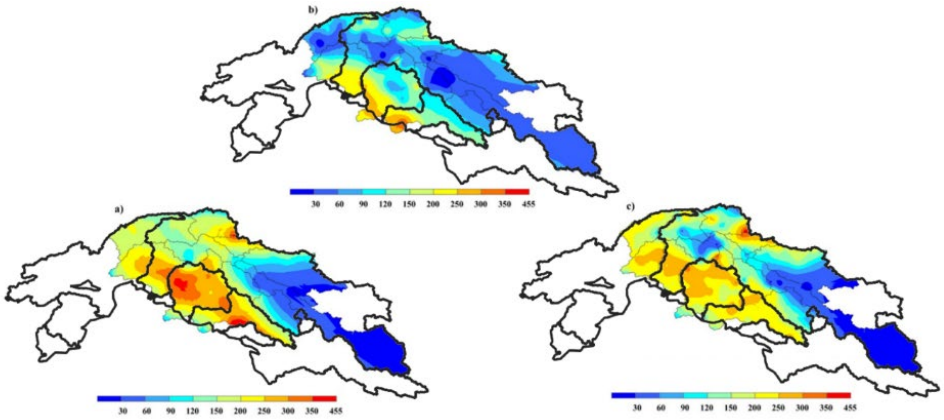

Figure 24: Precipitation (mm/year) over the UIB overlain by an outline of the rWTUs. a) April-June, b) July-September and c) October-March (Adapted from Dahri et al., 2016).

The snow indicator is highest for Kabul, Beas/Sutlej, and the Indus rWTU, while remaining low for the other rWTUs (Figure 19), which can largely be attributed to their lower interannual and intra-annual variability. Results from Immerzeel et al. (2009), displayed in Figure 3, show a high snow cover for all rWTUs, except Kurram/Tochi and Gumal. It thereby shows that parts of Kabul, the Indus rWTU, Chenab and Beas/Sutlej remain snow-covered throughout the entire year, resulting in a low intra-annual variability. Results from Lutz et al. (2014), displayed in Figure 25b, show that the snow runoff in all rWTUs amounts to approximately 500 mm/year, except for Kabul, the Indus rWTU and Jhelum, where the annual snow runoff can be up to 1000 mm/year. From these studies it becomes evident that the Indus rWTU and Kabul rank highest in the amount of snow, intra-annual and interannual variability. It also becomes evident that Beas/Sutlej and to a smaller extent Chenab score higher due to their low inter-annual and intra-annual variability, all consistent with previous findings.

The glacier indicator, displayed in Figure 19, has the highest values for Chenab and the Indus rWTU and to a smaller extent Kabul, mainly caused by the fraction of high glacial runoff to the total discharge. According to Lutz et al. (2014), the glacial runoff is highest in the Indus rWTU, Chenab and Beas/Sutlej, where the annual runoff can be as high as 2500 mm/year (Figure 25c). According to Pritchard (2019), the largest fraction of glacial melt can be found in the Indus rWTU and Chenab, followed by Kabul and Beas/Sutlej. These studies are consistent with the findings here. Beas/Sutlej has, however, received a slightly lower value than expected compared to the existing literature, likely due to the high intra-annual variability of the rWTU, which is not considered in the two studies. Biemans et al. (2019) found that the highest snow and glacier runoff stem from the Indus rWTU and Kabul, followed by Chenab and Beas/Sutlej (Figure 26). This is again consistent with the findings here.

Figure 19 displays that the highest surface water indicators are found in Beas/Sutlej, followed by the Indus rWTU and Ravi. According to a study by Ashraf et al. (2017), both non-glacial and glacial lakes in the Indus WTU can be found in rWTUs Kabul, Jhelum, and the Indus rWTU. This is further substantiated by Bolch et al. (2019) who found the largest lake volume to be in the Indus rWTU, Beas/Sutlej and Ravi. The findings done here do not completely coincide with the findings of Ashraf et al. (2017), however, do coincide with the findings of Bolch et al. (2019). Ashraf et al. (2017) solely studied Pakistan lakes, while Ravi and Beas/Sutlej lie in India, which can explain the different findings.

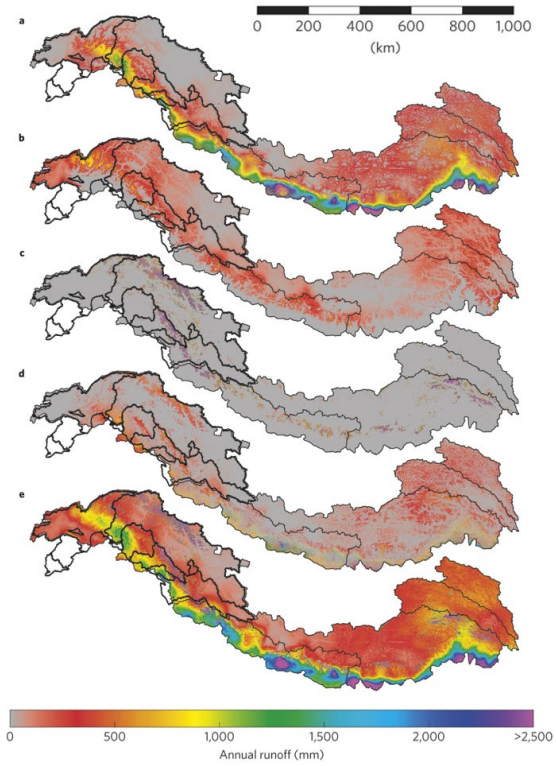

Figure 25: Annual runoff (mm/year) over the Indus Basin overlain by an outline of the rWTUs. a) rainfall runoff, b) snow runoff, c) glacial runoff, d) baseflow and e) total runoff (Adapted from Lutz et al., 2014).

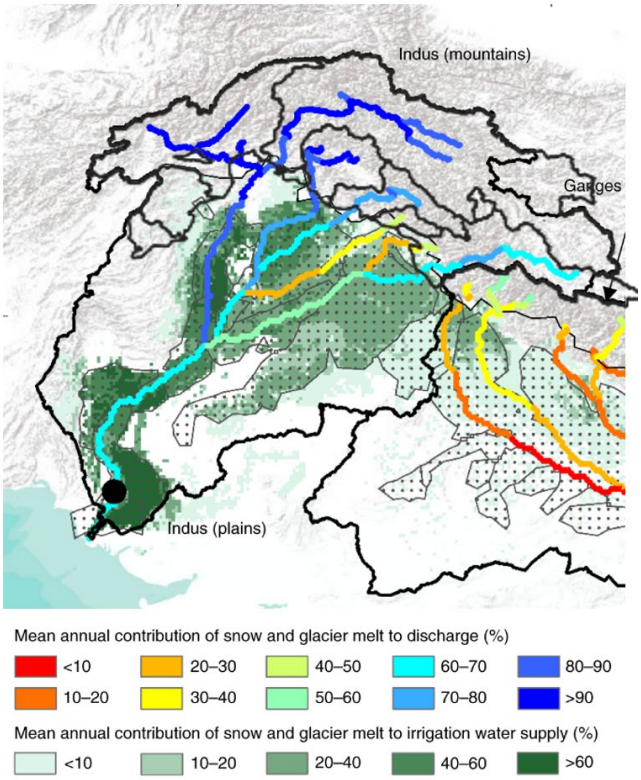

Figure 26: The contribution of snow and glaciers to discharge overlain by the outline of the rWTUs (Adapted from Biemans et al., 2019).

Figure 21 displays the highest SI-values for the Indus rWTU and Beas/Sutlej, while the lowest SI-values belong to Gumal and Kurram/Tochi. Lutz et al. (2014) found the total annual runoff to be highest in the Indus rWTU, Chenab, Beas/Sutlej and to a slightly lesser extent Kabul (Figure 25e). Wijngaard et al. (2018) found the largest supply to be in Beas/Sutlej, followed by Ravi, Jhelum and Chenab, Kabul, and the Indus rWTU (Figure 27). These two studies deviate largely in the importance of the Indus rWTU, even though it scores highest for the SI in this study. The importance of the other rWTUs does coincide with the studies, and the importance of the Indus rWTU is substantiated by Lutz et al. (2014).

Figure 20, displaying the demand indicators, shows that the industrial and domestic demand indicators are highest for Beas/Sutlej and Ravi, while being lowest for Gumal and Kurram/Tochi. There are little studies that research the water demand in the Indus Basin. Therefore, water consumption results from Wijngaard et al. (2018) are used as this can still give an indication of where the demand hotspots are located. Wijngaard et al. (2018) found that the highest domestic and industrial consumption is indeed located in the east of the Indus basin, while the lowest consumption occurs in the west (Figure 28). For the irrigation indicator, the same conclusion can be drawn, where Beas/Sutlej, Ravi, Chenab, Jhelum, and Kabul are hotspots. This can be explained by their high irrigation demand, causing a higher water gap, increasing the demand indicators. Overall, this corresponds well with Wijngaard et al. (2018).

The DI, displayed in Figure 21, shows an increased DI-value from west to east. This again corresponds with the findings by Wijngaard et al. (2018), where the water consumption increases from west to east for all sectors, especially for agriculture. The lowest consumption can indeed be found in Kurram/Tochi and Gumal.

Overall, the findings correspond well to the literature, where the overall rWTI is highest for the eastern rWTUs. This was expected as the highest DI-values are found here. Beas/Sutlej scores highest on the total rWTI, due to its various sources of supply and large water demand. The Indus subbasin scores highest on the SI, due to its large variation in sources, but scores lower on the rWTI due to its lower DI, again corresponding well to literature. Kurram/Tochi and Gumal score lowest for the SI due to their little variety in sources, consisting of mainly precipitation, and the low demand in the downstream areas, which corresponds well to literature.

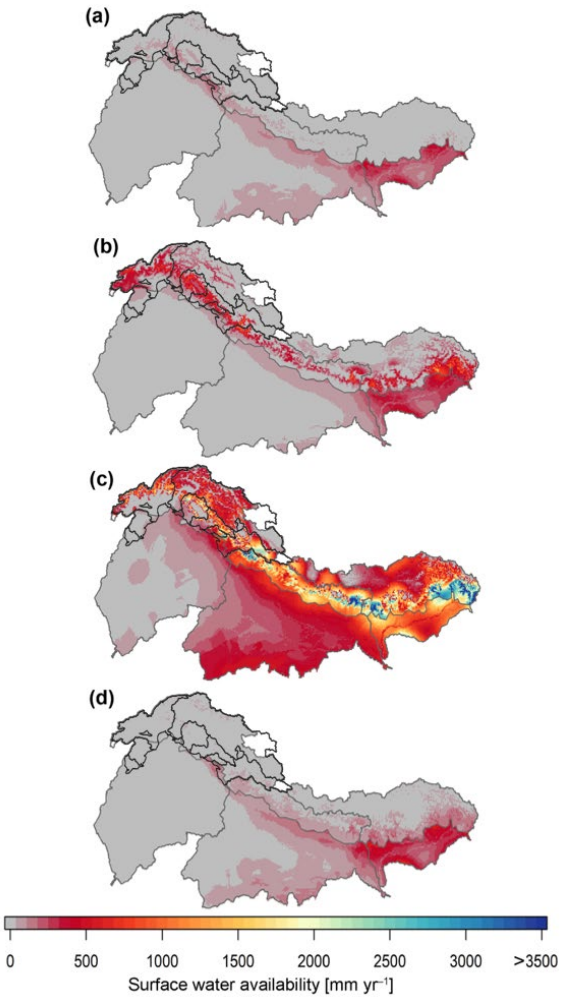

Figure 27: Surface water availability over the Indus Basin in a) winter, b) pre-monsoon, c) monsoon and d) post-monsoon seasons. This is overlain by an outline of the rWTUs (Wijngaard et al., 2018).

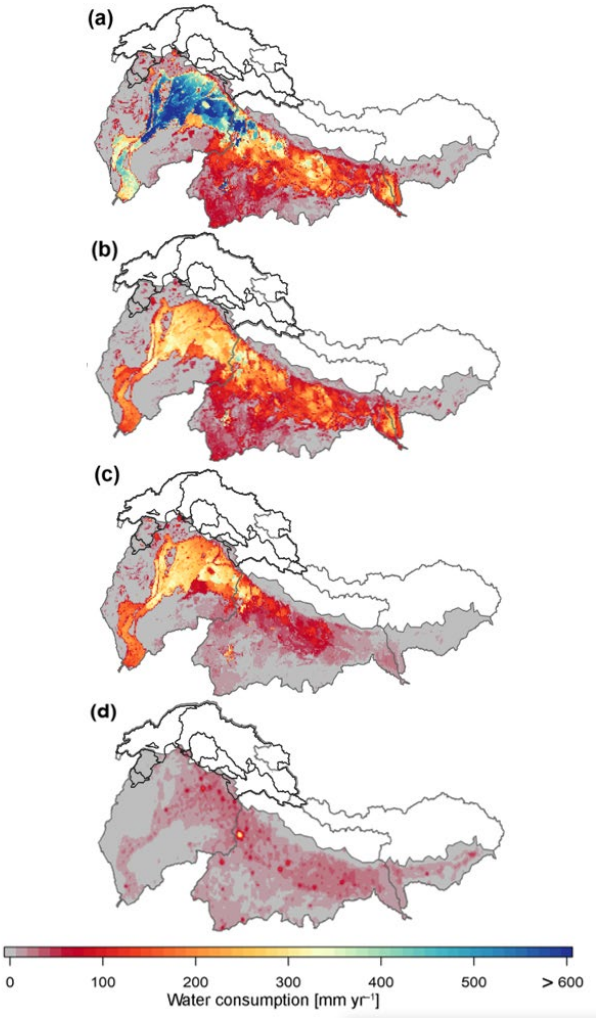

Figure 28: Water consumption over the Indus Basin overlain by an outline of the rWTUs. a) annual irrigation consumption, b) rabi seasons, c) kharif seasons and d) annual domestic + industrial water consumption (Wijngaard et al., 2018).

Figure 22c displays the highest water stress to occur in Beas/Sutlej and the Indus subbasin, while being lowest for Gumal, Chenab, Jhelum and Kurram/Tochi. When the units are changed to mm/year, Beas/Sutlej and Ravi score much higher than the other downstream areas. According to Wijngaard et al. (2018), Biemans et al. (2019), and Hofste et al. (2019), the highest unsustainable groundwater extraction occurs in Beas/Sutlej and Ravi (Figures 29, 30 and 31). What does stand out are the low scores for Chenab and Jhelum, which seem to deviate from findings done by the three studies. This, however, can be explained by the downstream areas of Chenab and Jhelum being the smallest, thereby leading to a lower sum.

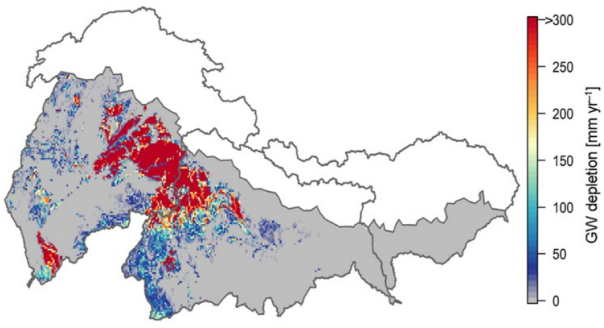

Figure 29: Groundwater depletion over the downstream Indus Basin (Wijngaard et al., 2018).

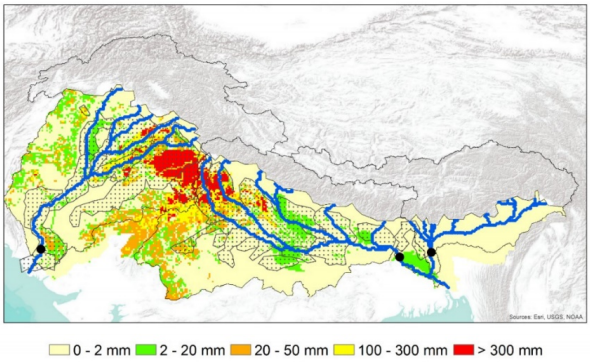

Figure 30: Groundwater depletion (mm/year) over the downstream Indus Basin (Biemans et al., 2019).

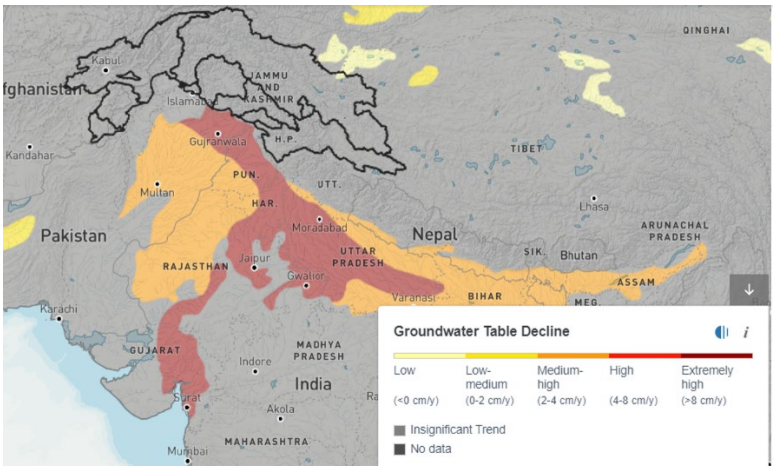

Figure 31: Unsustainable groundwater withdrawals over the downstream Indus Basin, overlain by an outline of the rWTUs (Adapted from Hofste et al., 2019).

4.4. Sensitivity to indicator weights

To ensure the reliability of the results, a sensitivity analysis on the indicator weights was performed. Figure 32 shows that the highest-scoring rWTU and the two lowest-scoring rWTUs solely shift no place in rank during 100% of the runs. The other five middle-to-high scoring rWTUs shift mostly 1 position in rank for 3.26% to 32.68% of the runs. Ravi and Kabul are the only rWTUs that shift more than 2 positions in rank, however this only occurs for 0.04 and 1.04% of the runs. The larger shift in rank for the middle-to-high scoring rWTUs could be due to the larger variation in sources compared to the lower rWTUs, causing them to be more vulnerable to different indicator weights. Overall, there is little change in positions and a low percentage of realizations when the rWTUs do shift. This displays a high robustness and reliability of the results.

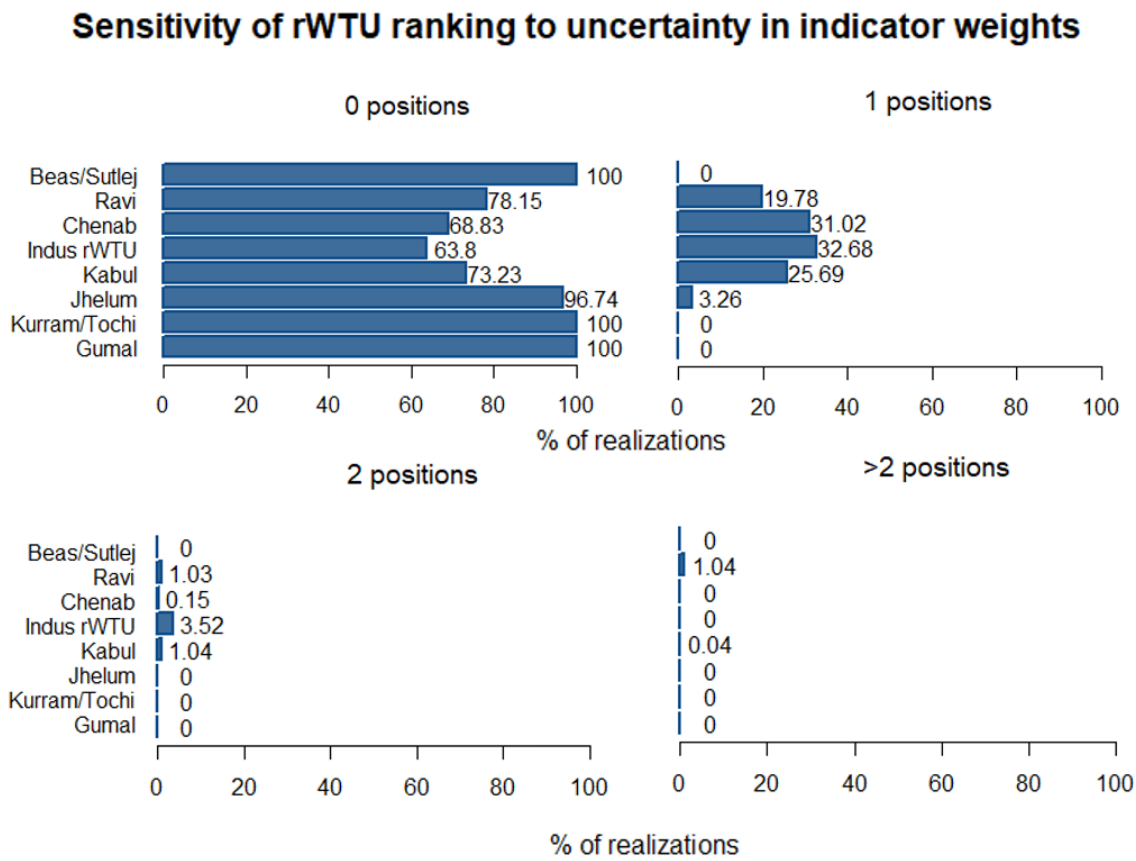

Figure 32: The sensitivity of the rWTU ranking to the uncertainty in indicator weights. The graphs show the number of positions each rWTU shifts, while the numbers in the graphs indicate the percentage of runs the position shift occurs in.

4.5. Limitations

This research contains several limitations, which could implicate the findings. First, there are limitations to the downstream area delineation. During the delineation, I chose to ignore small hydrological connections where only small parts of two subbasins were connected. Additionally, the man-made transfers of water between the subbasins in the IBIS are also not accounted for. Inclusion of these connections could have led to different results.

Second, there are limitations to the SI-formation. For the calculation of the regional SI, no regional precipitation data were used to avoid inconsistencies between precipitation and evaporation datasets (Section3.2.2). The inclusion of regional precipitation data could, however, have led to different outcomes. Thereby, the global precipitation data, used to calculate the regional SI, range from 2001-2014, while the regional snow and glacier data range from 1961-2007. This temporal shift could affect the outcomes of the SI. The calculation of the regional and global SI is also slightly different. For the regional SI, the glacier and snow indicators are not taken relative to the total precipitation, as for the global SI, but to the total runoff, which includes snowmelt, glacial melt, and rainfall. The regional snow and glacier indicator are therefore smaller as these are divided by more sources.

Third, there are limitations in determining the monthly water gaps for the DI. In this study, the downstream water supply is fully available to close the water gap for the different sectors. In practice, however, the sectors compete over this downstream water supply, increasing the water gap and thereby increasing the DI for each subbasin. Additionally, not all water generated within a subbasin is available for use within the entire subbasin, which could also impact the indicator outcomes.

Lastly, limitations are present in the used datasets. Some regional data are still missing, such as for the GE, where recent data is used instead of regional data. Additionally, different years are used for regional and global data to calculate the vulnerability to climate change, which gives an inconsistent comparison. Thereby, the global and regional climate datasets use different GCM runs, which can affect climate uncertainty and, therefore, the general outcome. Another data limitation is present due to data use from Lutz et al. (2016), who do not provide data on Gumal and only partly on Kurram/Tochi when calculating the regional glacier and snow indicators. These two rWTUs, however, score lowest on the glacier and snow indicators when using global data, thereby reducing the impact of this limitation.

4.6. Implications and future research

By building forward on the global WTI, proof is found that the rWTI has an improved representation of spatial variability compared to global scale assessments and is, therefore, of added value. Furthermore, by comparing the outcomes of the rWTI, formed with regional data, to other literature, it becomes evident that similar results to other hydrological studies can be obtained in a faster and less complex manner. This indicates that the rWTI-approach could function as a first estimate and an orientation tool for hydrological studies to determine the importance and vulnerability of a region. It is, however, recommended to perform this research for other basins than the Indus to obtain further evidence. This research does not solely contribute to the scientific literature, but also contributes to the knowledge base of the inhabitants, farmers, local political parties, and tourists of the Indus Basin. The results are especially important for the parties in Beas/Sutlej as this rWTU scores highest on the rWTI and water stress, while being the most important subbasin for food exportation (Wijngaard et al., 2018). It is, therefore, crucial that awareness is raised on the importance and vulnerability of Beas/Sutlej, however, this is also the case for the other rWTUs.

Water stress through unsustainable groundwater use is not solely important in Beas/Sutlej, but also occurs for many of the other rWTUs in the Indus Basin. The Indus Basin is extremely reliant on groundwater to close the water gaps (Archer et al., 2010; Cheema & Qamar, 2019). Groundwater has been considered in the VI but should for future research also be included as a fifth indicator in the SI and should be included in the DI to calculate the downstream water availability. Another improvement of the approach for future research could be obtained by including hydrological and water allocation model output in a water accounting framework. Water inputs can hereby be compared to water consumption, and reuse can also be accounted for.

5. Conclusion

In this study, I apply the global Water Tower Index (WTI) and Vulnerability Index (VI), developed by Immerzeel et al. (2020), at subbasin scale in the Indus Basin as there is a lack of an integrated view of all contributions to the water supply and demand at a scale smaller than the Water Tower Unit (WTU). This new approach is termed the regional Water Tower Index (rWTI), which is based on a Supply Index (SI) and Demand Index (DI) consisting of several indicators. The VI similarly consists of several static and dynamic indicators. Both global and regional data are used in this approach to enable a comparison to the findings by Immerzeel et al. (2020) and to hydrological studies performed at similar scale.

The results are subject to uncertainties; however, several conclusions can unambiguously be drawn. The results derived through global data first show large variability in the indicator outcomes for the eight delineated regional Water Tower Units (rWTUs), especially for the snow indicators, glacier indicators and DI-outcomes. The regional hydrological processes, such as the snow-albedo feedback in sustaining the snow cover due to low interannual and intra-annual variability, become visible in these outcomes. The outcomes derived by Immerzeel et al. (2020) for the total Indus Basin frequently take on the average value of the rWTU-outcomes. This, however, insufficiently considers the spatial variability, displaying the need for a regional approach to the global WTI.

When regional data is used over global data, the indicator outcomes of the rWTUs change in both value and ranking. This change is especially large for the vulnerability to water stress, the snow and glacier indicators and the DI. A significant finding is that for the DI-indicators, the importance of the upstream water supply in closing the water gaps becomes eminent. Significant changes also occur for the rWTI outcomes; when using global data, the Indus rWTU scores highest, whereas this is Beas/Sutlej when using regional data. Beas/Sutlej scores highest due to having the second-highest SI and having the highest DI, indicating it is the most important rWTU within the Indus Basin.

The results from the rWTI and VI derived through regional data coincide well with results drawn from other hydrological studies performed on subbasin scale. These findings hereby provide the first evidence that the global WTI-approach is applicable at subbasin scale, indicating that the regional Water Tower Index could be used as a first estimate and orientation tool to the more complex and time-consuming hydrological studies. More research on other basins globally is, however, required to provide further evidence on the applicability of the global WTI and VI at subbasin scale. Nevertheless, this research is useful in displaying the need to raise awareness on the importance and vulnerability of Beas/Sutlej for local political parties, inhabitants, tourists, and farmers.

6. References

Afzal, M. T., Arslan, M., Zafar, S., & Waqar, M. M. (2014). Satellite derived snow cover status and trends in the Indus Basin. *J Sp Technol*, *4*, 26-31.

Amin, A., Iqbal, J., Asghar, A., & Ribbe, L. (2018). Analysis of current and future water demands in the Upper Indus Basin under IPCC climate and socio-economic scenarios using a hydro-economic WEAP model. *Water, 10*(5), 537.

Archer, D. R., Forsythe, N., Fowler, H. J., & Shah, S. M. (2010). Sustainability of water resources management in the Indus Basin under changing climatic and socio economic conditions. *Hydrology and Earth System Sciences, 14*(8), 1669-1680.

Ashraf, A., Naz, R., & Iqbal, M. B. (2017). Altitudinal dynamics of glacial lakes under changing climate in the Hindu Kush, Karakoram, and Himalaya ranges. *Geomorphology*, *283*, 72-79.

Biemans, H., Siderius, C., Lutz, A. F., Nepal, S., Ahmad, B., Hassan, T., Von Bohl, W., Wijngaard, R. R., Wester, P., Shrestha, A. B., & Immerzeel, W. W. (2019). Importance of snow and glacier meltwater for agriculture on the Indo-Gangetic Plain. *Nature Sustainability, 2*(7), 594-601.

Bocchiola, D., & Soncini, A. (2019). Water Resources Modeling and Prospective Evaluation in the Indus River Under Present and Prospective Climate Change. In Khan, S. I., & Adams III, T. E. (Ed.), *Indus River Basin* (pp. 17-56). Amsterdam, The Netherlands: Elsevier.

Bolch, T. (2019). Past and Future Glacier Changes in the Indus River Basin. In Khan, S. I., & Adams III, T. E. (Ed.), *Indus River Basin* (pp. 85-94). Amsterdam, The Netherlands: Elsevier.

Bolch, T., Shea, J. M., Liu, S., Azam, F. M., Gao, Y., Gruber, S., Immerzeel, W. W., Kulkarni, A., Li, H., Tahir, A. A., Zhang, G., & Zhang, Y. (2019). Status and Change of the Cryosphere in the Extended Hindu Kush Himalaya Region. In Wester, P., Mishra, A., Mukherji, A. & Shrestha, A. B. (Ed.), *The Hindu Kush Himalaya Assessment* (pp. 211-257). Basel, Switzerland: Springer.

Cannon, F., Carvalho, L. M., Jones, C., & Norris, J. (2016). Winter westerly disturbance dynamics and precipitation in the western Himalaya and Karakoram: a wave-tracking approach. *Theoretical and Applied Climatology*, *125*(1), 27-44.

Cheema, M. J. M., Immerzeel, W. W., & Bastiaanssen, W. G. M. (2014). Spatial quantification of groundwater abstraction in the irrigated Indus basin. *Groundwater*, *52*(1), 25-36.

Cheema, M. J. M., & Qamar, M. U. (2019). Transboundary Indus River Basin: Potential Threats to Its Integrity. In Khan, S. I., & Adams III, T. E. (Ed.), *Indus River Basin* (pp. 183-201). Amsterdam, The Netherlands: Elsevier.

Climate data store. (n.d.). *Search results*. Retrieved from https://cds.climate.copernicus.eu/cdsapp#!/search?text=precipitation&type=dataset&keywords=((%20%22Product%20type:%20Reanalysis%22%20))

Dahri, Z. H., Ludwig, F., Moors, E., Ahmad, B., Khan, A., & Kabat, P. (2016). An appraisal of precipitation distribution in the high-altitude catchments of the Indus basin. *Science of the Total Environment, 548*, 289-306.

De Stefano, L., Petersen-Perlman, J. D., Sproles, E. A., Eynard, J., & Wolf, A. T. (2017). Assessment of transboundary river basins for potential hydro-political tensions. *Global Environmental Change*, *45*, 35-46.

Dingman, S. L. (2015). *Physical Hydrology*. United States, Illinois: Waveland Press, Inc.

DIVA-GIS. (2011). *Download data by country*. Retrieved from http://www.diva-gis.org/gdata

Farinosi, F., Giupponi, C., Reynaud, A., Ceccherini, G., Carmona-Moreno, C., De Roo, A., Gonzalez-Sanchez, D., & Bidoglio, G. (2018). An innovative approach to the assessment of hydro-political risk: A spatially explicit, data driven indicator of hydro-political issues. *Global Environmental Change*, *52*, 286-313.

Farinotti, D. (2019). *A consensus estimate for the ice thickness distribution of all glaciers on Earth – dataset.* Retrieved from https://www.research-collection.ethz.ch/handle/20.500.11850/315707

Farinotti, D., Huss, M., Fürst, J. J., Landmann, J., Machguth, H., Maussion, F., & Pandit, A. (2019). A consensus estimate for the ice thickness distribution of all glaciers on Earth. *Nature Geoscience, 12*(3), 168-173.

Gimond, M. (2021). *Intro to GIS and Spatial Analysis*. Retrieved from https://mgimond.github.io/Spatial/index.html

Gleeson, T., Wada, Y., Bierkens, M. F., & Van Beek, L. P. (2012). Water balance of global aquifers revealed by groundwater footprint. *Nature*, *488*(7410), 197-200.

Hall, D. K. & Riggs, G. A. (2021). *MODIS/Terra Snow Cover Monthly L3 Global 0.05Deg CMG, Version 61.* Boulder, Colorado USA. NASA National Snow and Ice Data Center Distributed Active Archive Center.

Hersbach, H., de Rosnay, P., Bell, B., Schepers, D., Simmons, A., Soci, C., Abdalla, S., Alonso-Balmaseda, M., Balsamo, G., Bechtold, P., Berrisford, P., Bidlot, J., De Boisséson, E., Bonavita, M., Browne, P., Buizza, R., Dahigren, P, Dee, D., Dragani, R., … & Zuo, H. (2018). *Operational global reanalysis: progress, future directions and synergies with NWP*. Retrieved from

https://www.ecmwf.int/en/elibrary/18765-operational-global-reanalysis-progress-future-directions-and-synergies-nwp

Hock, R., Rasul, G., Adler, C., Cáceres, B., Gruber, S., Hirabayashi, Y., Jackson, M., Kääb, A., Kang, S., Kutuzov, S., Milner, A., Molau, U., Morin, S., Orlove, B., & Steltzer, H. (2019). High Mountain Areas: In: IPCC Special Report on the Ocean and Cryosphere in a Changing Climate.

Hofste, R. W., Kuzma, S., Walker, S., Sutanudjaja, E. H., Bierkens, M. F. P., Kuijper, M. J., Sanchez, M. F., Van Beek, R., Wada, Y., Rodríguez, S. G., & Reig, P. (2019). Aqueduct 3.0: Updated Decision-Relevant Global Water Risk Indicators. *World Resources Institute: Washington, DC, USA*.

Houze Jr, R. A., Wilton, D. C., & Smull, B. F. (2007). Monsoon convection in the Himalayan region as seen by the TRMM Precipitation Radar. *Quarterly Journal of the Royal Meteorological Society: A journal of the atmospheric sciences, applied meteorology and physical oceanography, 133*(627), 1389-1411.

Hussain, I., Hussain, Z., Sial, M. H., Akram, W., & Farhan, M. F. (2011). Water balance, supply and demand and irrigation efficiency of Indus Basin. *Pakistan Economic and Social Review*, 13-38.

Huss, M., Bookhagen, B., Huggel, C., Jacobsen, D., Bradley, R. S., Clague, J. J., Vuille, M., Buytaert, W., Cayan, D. R., Greenwood, G., Mark, B. G., Milner, A. M., Weingartner, R., & Winder, M. (2017). Toward mountains without permanent snow and ice. *Earth's Future*, *5*(5), 418-435.

HydroSHEDS. (n.d.-a). *HydroBASINS Version 1.0.* Retrieved from https://www.hydrosheds.org/page/hydrobasins

HydroSHEDS. (n.d.-b). *HydroLAKES Version 1.0.* Retrieved from https://www.hydrosheds.org/pages/hydrolakes

Immerzeel, W. W., Droogers, P., De Jong, S. M., & Bierkens, M. F. P. (2009). Large-scale monitoring of snow cover and runoff simulation in Himalayan river basins using remote sensing. *Remote sensing of Environment, 113*(1), 40-49.

Immerzeel, W. W., Lutz, A. F., Andrade, M., Bahl, A., Biemans, H., Bolch, T., Hyde, S., Brumby, S., Davies, B. J., Elmore, A. C., Emmer, A., Feng, M., Fernández, A., Haritashya, U., Kargel, J. S., Koppes, M., Kraaijenbrink, P. D. A., Kulkarni, A. V., Mayewski, P. A., … & Baillie, J. E. M. (2020). Importance and vulnerability of the world's water towers. *Nature, 577*(7790), 364-369.

Immerzeel, W. W., Van Beek, L. P., & Bierkens, M. F. (2010). Climate change will affect the Asian water towers. *Science, 328*(5984), 1382-1385.

Immerzeel, W. W., Wanders, N., Lutz, A. F., Shea, J. M., & Bierkens, M. F. P. (2015). Reconciling high-altitude precipitation in the upper Indus basin with glacier mass balances and runoff. *Hydrology and Earth System Sciences, 19*(11), 4673-4687.

Kaufmann, D., Kraay, A., & Mastruzzi, M. (2010). *The worldwide governance indicators: methodology and analytical issue*. Retrieved from https://info.worldbank.org/governance/wgi/Home/Documents

Kauffman, D. & Kraay, A. (2019). *Worldwide Governance Indicators.* Retrieved from https://info.worldbank.org/governance/wgi/

Khan, A. J., & Koch, M. (2018). Correction and informed regionalization of precipitation data in a high mountainous region (Upper Indus Basin) and its effect on SWAT-modelled discharge. *Water*, *10*(11), 1557.

Khan, A., Richards, K. S., Parker, G. T., McRobie, A., & Mukhopadhyay, B. (2014). How large is the Upper Indus Basin? The pitfalls of auto-delineation using DEMs. *Journal of Hydrology*, *509*, 442-453.

Khan, F., Pilz, J., & Ali, S. (2017). Improved hydrological projections and reservoir management in the Upper Indus Basin under the changing climate. *Water and Environment Journal, 31*(2), 235-244.

Kiani, A., Ijaz, F., & Siddique, H. M. A. (2018). Determinants of Agricultural Exports of Pakistan: An Application of Gravity Model. *Dialogue (Pakistan)*, *13*(4).

KNMI. (2020). *Select a monthly field.* Retrieved from https://climexp.knmi.nl/selectfield_cmip5.cgi?id=someone@somewhere

Koppes, M., Rupper, S., Asay, M., & Winter-Billington, A. (2015). Sensitivity of glacier runoff projections to baseline climate data in the Indus River basin. *Frontiers in Earth Science*, *3*, 59.

Krishnan, R., Shrestha, A. B., Ren, G., Rajbhandari, R., Saeed, S., Sanjay, Abu Syed, M., Vellore, R., Xu, Y., You, Q., & Ren, Y. (2019). Unravelling climate change in the Hindu Kush Himalaya: Rapid warming in the mountains and increasing extremes. In Wester, P., Mishra, A., Mukherji, A. & Shrestha, A. B. (Ed.), *The Hindu Kush Himalaya Assessment* (pp. 57-91). Basel, Switzerland: Springer.

Laghari, A. N., Vanham, D., & Rauch, W. (2012). The Indus basin in the framework of current and future water resources management. *Hydrology and Earth System Sciences*, *16*(4), 1063-1083.

Lehner, B., & Grill, G. (2013). Global river hydrography and network routing: baseline data and new approaches to study the world's large river systems. *Hydrological Processes, 27*(15), 2171–2186.

Lehner, B. & Messager. M. (2016). *HydroLAKES: Technical documentation version 1.0*. Retrieved from https://www.hydrosheds.org/images/inpages/HydroLAKES_TechDoc_v10.pdf

Liu, W., Xie, C., Zhao, L., Li, R., Liu, G., Wang, W., Liu, H., Wu, T., Yang, G., Zhang, Y., & Zhao, S. (2021). Rapid expansion of lakes in the endorheic basin on the Qinghai-Tibet Plateau since 2000 and its potential drivers. *CATENA*, *197*, 104942.

Li, Y., Su, F., Chen, D., & Tang, Q. (2019). Atmospheric water transport to the endorheic Tibetan plateau and its effect on the hydrological status in the region. *Journal of Geophysical Research: Atmospheres*, *124*(23), 12864-12881.

Lund, J., Forster, R. R., Rupper, S. B., Deeb, E. J., Marshall, H. P., Hashmi, M. Z., & Burgess, E. (2020). Mapping snowmelt progression in the Upper Indus Basin with synthetic aperture radar. *Frontiers in Earth Science*, *7*, 318.

Lutz, A. F., Immerzeel, W. W., Kraaijenbrink, P. D., Shrestha, A. B., & Bierkens, M. F. (2016). Climate change impacts on the upper indus hydrology: Sources, shifts and extremes. *PloS one, 11*(11).

Lutz, A. F., Immerzeel, W. W., Shrestha, A. B., & Bierkens, M. F. P. (2014). Consistent increase in High Asia's runoff due to increasing glacier melt and precipitation. *Nature Climate Change, 4*(7), 587-592.

Medina, S., Houze Jr, R. A., Kumar, A., & Niyogi, D. (2010). Summer monsoon convection in the Himalayan region: Terrain and land cover effects. *Quarterly Journal of the Royal Meteorological Society: A journal of the atmospheric sciences, applied meteorology and physical oceanography, 136*(648), 593-616.

Mesquita, M. D. S., Orsolini, Y. J., Pal, I., Veldore, V., Li, L., Raghavan, K., Panandiker, A. M., Honnungar, V., Gochis, D., & Burkhart, J. F. (2019). Challenges in Forecasting Water Resources of the Indus River Basin: Lessons From the Analysis and Modeling of Atmospheric and Hydrological Processes. In Khan, S. I., & Adams III, T. E. (Ed.), *Indus River Basin* (pp. 57-79). Amsterdam, The Netherlands: Elsevier.

Messerli, B., Viviroli, D., & Weingartner, R. (2004). Mountains of the world: vulnerable water towers for the 21st century. *AMBIO: A Journal of the Human Environment, 33*(sp13), 29-34.

Mukherji, A., Scott, C., Molden, D., & Maharjan, A. (2018). Megatrends in Hindu Kush Himalaya: Climate change, urbanisation and migration and their implications for water, energy and food. In *Assessing global water megatrends* (pp. 125-146). Springer, Singapore.

Murakami, D., & Yamagata, Y. (2019). Estimation of gridded population and GDP scenarios with spatially explicit statistical downscaling. *Sustainability, 11*(7), 2106.

Pepin, N., Bradley, R. S., Diaz, H. F., Baraër, M., Caceres, E. B., Forsythe, N., Fowler, H., Greenwood, G., Hashmi, M. Z., Liu, X. D., Miller, J. R., Ning, L., Ohmura, A., Palazzi, E., Rangwala, I., Schöner, W., Severskiy, I., Shahgedanova, M., Wang, M. B., … & Yang. D. Q. (2015). Elevation-dependent warming in mountain regions of the world. *Nature climate change*, *5*(5), 424.

Pritchard, H. D. (2019). Asia's shrinking glaciers protect large populations from drought stress. *Nature, 569*(7758), 649-654.

Qureshi, A. S., McCornick, P. G., Sarwar, A., & Sharma, B. R. (2010). Challenges and prospects of sustainable groundwater management in the Indus Basin, Pakistan. *Water resources management*, *24*(8), 1551-1569.

Qureshi, W. A. (2018). Dispute resolution mechanisms: An analysis of the indus waters treaty. *Pepp. Disp. Resol. LJ*, *18*, 75-110.

Rasheed, B. (2013). *Impact assessment of hydroclimatic change on water stress in the Indus Basin* (Doctoral dissertation, Massachusetts Institute of Technology).

Resource Watch. (2019). *Hydropolitical Tension and Institutional Vulnerability.* Retrieved from Hydropolitical Tension and Institutional Vulnerability | Resource Watch

Saqib Riaz, D., Ishaque, W., & Baig, M. A. (2020). Indian aqua aggression: investigation the impact of Indus Water Treaty (IWT) on future of India-Pakistan water dispute. *NDU Journal*, 131-146.

Scott, C. A., Zhang, F., Mukherji, A., Immerzeel, W., Mustafa, D., & Bharati, L. (2019). Water in the Hindu Kush Himalaya. In Wester, P., Mishra, A., Mukherji, A. & Shrestha, A. B. (Ed.), *The Hindu Kush Himalaya Assessment* (pp. 258-292). Basel, Switzerland: Springer.

Shah, M. I., Khan, A., Akbar, T. A., Hassan, Q. K., Khan, A. J., & Dewan, A. (2020). Predicting hydrologic responses to climate changes in highly glacierized and mountainous region Upper Indus Basin. *Royal Society open science, 7*(8), 191957.

Shrestha, A. B., Wagle, N., & Rajbhandari, R. (2019). A review on the projected changes in climate over the Indus Basin. *Indus River Basin*, 145-158.

Smakhtin, V., Revenga, C., & Döll, P. (2004). A pilot global assessment of environmental water requirements and scarcity. *Water International*, *29*(3), 307-317.

Smolenaars, W., Lutz, A., Biemans., H., Dhaubanjar, S., Immerzeel, W., & Ludwig, F. (under review). *From narratives to numbers; spatial downscaling and quantification of future water-, food-& energy- security requirements in the Indus basin*.

Thackeray, C. W., Derksen, C., Fletcher, C. G., & Hall, A. (2019). Snow and climate: feedbacks, drivers, and indices of change. *Current Climate Change Reports, 5*(4), 322-333.

UNEP-DHI & UNEP. (2016). *Transboundary River Basins: Status and Trends.* Retrieved from https://transboundarywaters.science.oregonstate.edu/sites/transboundarywaters.science.oregonstate.edu/files/Database/ResearchProjects/TWAP/GEF_TWAPRB_FullTechnicalReport_compressed.pdf

United Nations. (2018). *Maps.* Retrieved from https://population.un.org/wup/Maps/

Viviroli, D., Archer, D. R., Buytaert, W., Fowler, H. J., Greenwood, G. B., Hamlet, A. F., Huang, Y., Koboltschnig, G., Litaor, M. I., López-Moreno, J. I., Lorentz, S., Schädler, B., Schreier, H., Schwaiger, K., Vuille, M., & Woods, R. (2011). Climate change and mountain water resources: overview and recommendations for research, management and policy. *Hydrology and Earth System Sciences*, *15*(2), 471-504.

Viviroli, D., Dürr, H. H., Messerli, B., Meybeck, M., & Weingartner, R. (2007). Mountains of the world, water towers for humanity: Typology, mapping, and global significance. *Water resources research, 43*(7).

Viviroli, D., Kummu, M., Meybeck, M., Kallio, M., & Wada, Y. (2020). Increasing dependence of lowland populations on mountain water resources. *Nature Sustainability*, *3*(11), 917-928.

Viviroli, D., Messerli, B., Schädler, B., & Weingartner, R. (2009). *Water towers in a changing world.* Retrieved from https://boris.unibe.ch/36487/1/Seiten%20aus%20Fullversion_low_Mountains_and%20_Climate_Change.pdf

Wada, Y., de Graaf, I. E., & van Beek, L. P. (2016). High-resolution modeling of human and climate impacts on global water resources. *Journal of Advances in Modeling Earth Systems*, *8*(2), 735-763.

Wang, Y., Wu, N., Kunze, C., Long, R., & Perlik, M. (2019). Drivers of change to mountain sustainability in the Hindu Kush Himalaya. In Wester, P., Mishra, A., Mukherji, A. & Shrestha, A. B. (Ed.), *The Hindu Kush Himalaya Assessment* (pp. 18-45). Basel, Switzerland: Springer.

Wescoat Jr, J. L., Halvorson, S. J., & Mustafa, D. (2000). Water management in the Indus basin of Pakistan: a half-century perspective. *International Journal of Water Resources Development*, *16*(3), 391-406.

WGMS. (2020). *Fluctuations of Glaciers Database. World Glacier Monitoring Service, Zurich, Switzerland.* Retrieved from http://dx.doi.org/10.5904/wgms-fog-2020-08

Wijngaard, R. R., Biemans, H., Lutz, A. F., Shrestha, A. B., Wester, P., & Immerzeel, W. W. (2018). Climate change vs. socio-economic development: understanding the future South Asian water gap. *Hydrology and Earth System Sciences*, *22*(12), 6297-6321.

Wijngaard, R. R., Lutz, A. F., Nepal, S., Khanal, S., Pradhananga, S., Shrestha, A. B., & Immerzeel, W. W. (2017). Future changes in hydro-climatic extremes in the Upper Indus, Ganges, and Brahmaputra River basins. *PloS one, 12*(12).

Wolledge, P. (2012, June 24). *Indus & Zanskar river confluence. Winter*. Retrieved from https://www.pbase.com/asiatramp/image/115470679

Zhang, G., Yao, T., Shum, C. K., Yi, S., Yang, K., Xie, H., Feng, W., Bolch, T., Wang, L., Behrangi, A., Zhang, H., Wang, Wl., Xiang, Y., & Yu, J. (2017). Lake volume and groundwater storage variations in Tibetan Plateau's endorheic basin. *Geophysical Research Letters*, *44*(11), 5550-5560.

Annex I

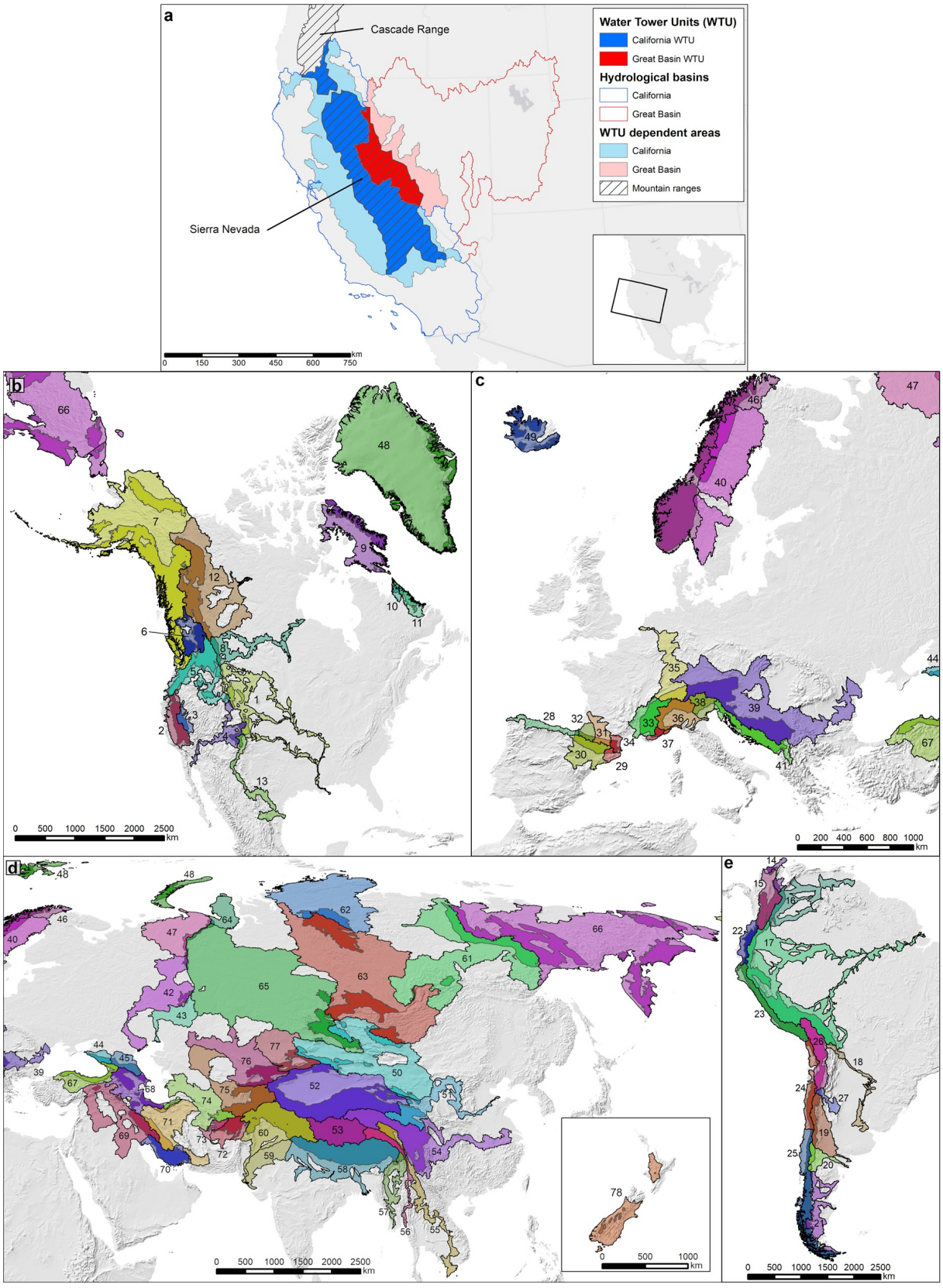

Figure 33: The global Water Tower Units (WTUs) are shown in the darker colours, while their downstream areas are shown in lighter colours. Immerzeel et al. (2020) define WTUs as the intersection of hydrological basins and mountain ranges that meet certain cryosphere thresholds (Annex II). This implies that one WTU can contain multiple mountain ranges. The downstream area consists of the subbasins within the hydrological basin that are hydrologically connected to that WTU and hydrologically connected to each other. The Indus Basin is represented by number 60 (Immerzeel et al. (2020).

Annex II

Table 5: An overview of the global and regional datasets used to calculate each indicator.

Section	Required data	Description of global data	Source of global data	Description of regional and/or more recent data	Source of regional data
Delineation of rWTUs and downstream areas	Mountain regions with certain glacier/ snow criteria	GMBA_all: This dataset of Immerzeel et al. (2020) contains mountain region that have an ice volume/area larger than 0.1 km^3/km^2 or that have an average annual areal snow persistence larger than 10%. Solely the mountain regions that met these remained in the dataset.	-Immerzeel et al., 2020	N.R.	N.R.
	Hydrological basins in Southeast Asia	N.R.	N.R.	HydroBASINS: This dataset divides Southeast Asia in major basins of which one is the Indus and subdivides these into smaller subbasins. This subdivision is done according to the Pfafstetter concept and level 6 of this division is used to delineate the subbasins.	-HydroSHEDS, n.d-a. -Lehner& Grill, 2013
	Indus waterways displaying hydrological connections	N.R.	N.R.	DIVA-GIS: This dataset displays the waterways of Pakistan, Afghanistan, India, and China in a shapefile. It is originally derived from the Digital Chart of the World, produced by the United States Defense Mapping Agency.	-DIVA-GIS, 2011
	Annual and monthly precipitation amount	ERA5 reanalysis: Annual and monthly precipitation data are derived from the ERA5 reanalysis, which reanalyses atmosphere, land and oceans through observations and models.	-Hersbach et al., 2018 -Climate data store, n.d.	N.A. Precipitation data in the downstream areas need to be used in combination with evaporation data (Section 3.2.3.). As there are no downscaled coupled precipitation-evaporation data available, no regional precipitation dataset is used.	N.A.

Supply Index	Snow cover and snowmelt	MODIS: This dataset contains the average yearly and monthly mean snow cover in a 0.05-degree resolution. It was acquired through the Earth Observing System, containing satellites and sensors.	- Hall & Riggs, 2021	Lutz et al., 2016: Through a high-resolution and raster based SPHY model the total runoff is calculated for the UIB in this dataset. The fraction of glacial meltwater and snowmelt to this total runoff is determined. It is made available in map-format for yearly data and in tss-format for monthly data. Both glacial melt and snowmelt have been determined through degree-day modelling, where debris, groundwater recharge and refreezing are considered.	-Lutz et al., 2016
	Glacial volume, area, mass balance and meltwater	Farinotti, 2019: Glacial volume and area data were acquired through five ice thickness estimation models. The mass balance changes are collected from the world glacier monitoring service (WGMS), which were acquired through in-situ observations and remote sensing.	-Farinotti, 2019 -Farinotti et al., 2019 -WGMS, 2020		
	Lakes and reservoirs	HydroLAKES: It displays polygons of all lakes with a surface area of more than 10 ha. The names, country, continent, type of lake, volume, area, id, elevation, and depth of the lakes are given.	-Lehner & Messager, 2016 -HydroSHEDS, n.d.-b	HydroLAKES: The same dataset is used as for the global approach, however now filtered on having an average long-term discharge of 0.00 m^3/s. This ensures solely exorheic lakes are included.	-Lehner & Messager, 2016 -HydroSHEDS, n.d.-b
Demand Index	Monthly and annual domestic, irrigation and industrial demand	Human water demand: These data are derived by Immerzeel et al. (2020) but have been made available by Wada et al. (2016). The dataset has a global extent, ranges from 1959 to 2014 and is given in $km^3\ yr^{-1.}$	-Immerzeel et al., 2020 -Wada, De Graaf & van Beek, 2016	N.A.	N.A.
	Monthly and annual environmental flow requirement	Natural flow demand: This data was estimated with the 90-th percentile exceedance value of natural flow. The water demand dataset has a global extent and is given in m^3/s.	-Immerzeel et al., 2020 - Wada, De Graaf & van Beek, 2016 -Gleeson, Wada, Bierkens & Van Beek, 2012 -Smakhtin, Revenga & Döll, 2004	N.A.	N.A.
	Annual/monthly precipitation and evaporation	ERA5 reanalysis: Annual and monthly precipitation and evaporation data are derived from	-Hersbach et al., 2018 -Climate data store, n.d.	N.A. See explanation above for the precipitation indicator in Supply Index.	N.A.

	the ERA5 reanalysis, which reanalyses atmosphere, land and oceans through observations and models.			
Total runoff supplied by the rWTUs to the downstream area	N.R.	N.R.	Lutz et al., 2016: Through a high-resolution and raster based SPHY model the total runoff is calculated for the UIB.	-Lutz et al., 2016
Government effectiveness	Worldwide governance indicators: This dataset contains government effectiveness, which entails the quality of public services, civil service, policy formulation and implementation. It also includes independence from political pressures and credibility of government's commitments to policies. The GE values of 2018 are used.	-Kaufmann & Kraay, 2019 -Kaufmann, Kraay & Mastruzzi, 2010	Worldwide governance indicators: The same dataset as for the global approach is used, however, now for the year 2019.	-Kaufmann & Kraay, 2019 -Kaufmann, Kraay & Mastruzzi, 2010
Hydro-political tension	UNEP-DHI & UNEP, 2016: This dataset displays hydro-political tension for each major basin on a scale from 1 to 5, where 1 indicates a very low risk for hydro-political tension and 5 indicates a very high risk. The hydro-political tension is calculated based on infrastructural development of a basin in the absence of institutional capacity.	-Resource Watch, 2019 -UNEP-DHI & UNEP, 2016	Transboundary Freshwater Dispute Database: A similar dataset is used as for the global approach, however, this dataset also displays certain subbasins. The scale levels and the manner in which it is calculated are similar to the global dataset.	-Resource Watch, 2019 -UNEP-DHI & UNEP, 2016
Water stress; global baseline water stress and regional unsustainable groundwater extraction.	Aqueduct: The BWS entails the ratio between the available renewable surface water and groundwater supplies and includes water withdrawals from the different sectors. BWS values for 2014 are used.	-Hofste et al., 2019 -Immerzeel et al., 2020	Biemans et al., 2019: The unsustainable groundwater extraction data (mm) contain solely the downstream areas of the Indus Basin. A LPJmL model was used, where water supply by upstream sources is modelled to meet the irrigation demand. If this demand cannot be met, the water is withdrawn from groundwater and when this extraction exceeds the recharge rate the groundwater extraction becomes unsustainable.	-Biemans et al., 2019
Population projections	HYDE dataset: Population projections in millions are given for SSP1, SSP2 and SSP3 globally and were downscaled by country into a 0.5-degree grid.	-Murakami & Yamagata, 2019	Smolenaars et al. (under review): This dataset contains population projections specifically for the Indus region. The projections build forth on the SSP	Smolenaars et al., under review

Vulnerability Index		Downscaling was done by using dasymetric mapping. Population values are given for the years 2000 and 2016 for SSP2 and 2050 for SSP1, SSP2 and SSP3.		projections, however, were downscaled by a newly developed BasinPop model. This model contains a large range of explanatory variables and spatial layers of boundary conditions to create a suitability map. The model runs on a 5 arcmin resolution.	
	GDP projections	HYDE dataset: GDP projections in billion US$ per year are given for SSP1, SSP2 and SSP3 globally and were downscaled by country into a 0.5-degree grid. Downscaling was done by using dasymetric mapping. GDP values are given for the year 2000 and 2016 for SSP2 and 2050 for SSP1, SSP2, SSP3.	-Murakami & Yamagata, 2019	Smolenaars et al. (under review): This dataset contains population projections multiplied by the GDP of the Indus region to obtain GDP projections. The projections build forth on the SSP projections, however, were downscaled by a newly developed BasinPop model. This model contains a large range of explanatory variables and spatial layers of boundary conditions to create a suitability map. The model runs on a 5 arcmin resolution.	Smolenaars et al., under review
	Precipitation and temperature projections of RCP4.5 and RCP8.5	A. Lutz: 35 RCP4.5 and 32 RCP8.5 GCM runs (CMIP5) are derived from A. Lutz for the UIB from 2036-2065 compared to 1986-2015. The included runs are visible in Table 3.	-KNMI, 2020	Lutz et al., 2016: Four RCP4.5 and four RCP8.5 downscaled GCM runs are available for the UIB from 2071-2100 compared to 1971–2000. The runs were downscaled using the Advanced Delta Change method, based on the entire precipitation distribution. The included runs are visible in Table 4.	-Lutz et al., 2016

N.A.=Not available
N.R.=Not required, as global data or regional data can be used for this purpose

Annex III

Table 6: An overview of the equations to calculate the rWTI both with global and regional data (Adapted from Immerzeel et al., 2020).

Section	Indicator	Symbol	Input	Equation
Global Supply Index	Precipitation contribution to rWTU/subbasin	P_T	Average annual rWTU precipitation sum (2001-2017): P_{rWTU} (km^3) Average annual subbasin precipitation sum (2001-2017): P_{SUBBAS} (km^3)	$P_T=P_{rWTU}/P_{SUBBAS}$
	Interannual variability in precipitation	P_{YV}	Annual rWTU precipitation for individual years (2001-2017): P_y (km^3)	$P_{YV}=1-((max(P_y)-min(P_y))/max(P_y)$
	Intra-annual variability in precipitation	P_{MV}	Average monthly rWTU precipitation sum (2001-2017): P_m (km^3)	$P_{MV}=1-((max(P_m)-min(P_m))/max(P_m)$
	Precipitation	P	-	$P=0.5*(P_{YV}+P_{MV})*P_T$
	rWTU snow cover	S_T	Average annual rWTU snow cover: S (-)	-
	Interannual variability in snow cover	S_{YV}	Annual average rWTU snow cover (2001-2017): S_y (-)	$S_{YV}=1-((max(S_y)-min(S_y))/max(S_y)$
	Intra-annual variability in snow cover	S_{MV}	Average monthly snow cover (2001-2017): S_m (-)	$S_{MV}=1-((max(S_m)-min(S_m))/max(S_m)$
	Snow	S_g	-	$S_g=0.5*(S_{YV}+S_{MV})*S_T$

Glacier ice storage	G_S	Total glacier ice volume in rWTU: G_V (km^3) Average annual rWTU precipitation sum (2001-2017): P_{rWTU} (km^3)	$G_S=G_V/(G_V+P_{rWTU})$
Glacier water yield	G_Y	Average annual rWTU precipitation sum (2001-2017): P_{rWTU} (km^3) Average annual precipitation sum glaciated area (2001-2017): P_{GLAC} (km^3) Average annual glacier mass balance of rWTU: B (km^3)	$G_Y=(P_{GLAC}-B)/(P_{GLAC}-B+P_{rWTU})$
Glaciers	G_g	-	$G_g=(G_s+G_Y)/2$
Surface waters	L_g	Total volume stored in lakes and reservoirs in rWTUs: S_L (km^3) Average annual rWTU precipitation sum (2001-2017): P_{rWTU} (km^3)	$L_g=S_L/(S_L+P_{rWTU})$
Global Supply Index	SI_g	-	$(P+S_g+G_g+L_g)/4$
Precipitation contribution to rWTU/subbasin	P_T	Average annual rWTU precipitation sum (2001-2017): P_{rWTU} (km^3) Average annual subbasin precipitation sum (2001-2017): P_{SUBBAS} (km^3)	$P_T=P_{rWTU}/P_{SUBBAS}$

Regional Supply Index	Interannual variability in precipitation	P_{YV}	Annual rWTU precipitation for individual years (2001-2017): P_y (km^3)	$P_{YV}=1-((max(P_y)-min(P_y))/max(P_y)$
	Intra-annual variability in precipitation	P_{MV}	Average monthly rWTU precipitation sum (2001-2017): P_m (km^3)	$P_{MV}=1-((max(P_m)-min(P_m))/max(P_m)$
	Precipitation	P	-	$P=0.5*(P_{YV}+P_{MV})*P_T$
	Interannual variability snow	S_{YV}	Annual rWTU snow runoff for individual years (1961-2007): $Q_{S,y}$ (km^3/year)	$S_{YV}=1-((max(Q_{S,y})-min(Q_{S,y}))/max(Q_{S,y})$
	Intra-annual variability snow	S_{MV}	Average monthly rWTU snow runoff (1961-2007): $Q_{S,m}$ (km^3/month)	$S_{MV}=1-((max(Q_{S,m})-min(Q_{S,m}))/max(Q_{S,m})$
	Snow	S_r	Maximum routed annual rWTU runoff (1961-2007): Q_{rWTU} (km^3)	$S_r=(0.5*(S_{YV}+S_{MV}))*(Q_S/Q_{rWTU})$
			Maximum routed annual snow runoff (1961-2007) in rWTU: Q_S (km^3)	
	Interannual variability glaciers	G_{YV}	Annual rWTU glacial runoff for individual years (1961-2007): $Q_{G,y}$ (km^3/year)	$G_{YV}=1-((max(Q_{G,y})-min(Q_{G,y}))/max(Q_{G,y})$
	Intra-annual variability glaciers	G_{MV}	Average monthly rWTU glacier runoff (1961-2007): $Q_{G,m}$ (km^3/month)	$G_{MV}=1-((max(Q_{G,m})-min(Q_{G,m}))/max(Q_{G,m})$
	Glaciers	G_r	Maximum routed annual rWTU runoff (1961-2007): Q_{rWTU} (km^3)	$G_r = (0.5*(G_{YV}+G_{MV}))*(Q_G/Q_{rWTU})$
			Maximum routed annual glacier runoff (1961-2007) in rWTU: Q_G (km^3)	
	Surface waters	L_r	Total volume stored in lakes and reservoirs connected to the river systems in rWTUs: $S_{L,con}$ (km^3)	$L_r=S_{L,con}/(S_{L,con}+P_{rWTU})$

			Average annual rWTU precipitation sum (2001-2017): P_{rWTU} (km^3)	
	Regional Supply Index	SI_r	-	$(P+S_r+G_r+L_r)/4$
Global Demand Index	Irrigation demand	$D_{IRR,g}$	Average annual downstream irrigation water use (2001-2014): $D_{IRR,y}$ (km^3)	$\sum(D_{IRR,m} - WA_{IRR,m})/D_{IRR,y}$
			Average monthly downstream irrigation water use (2001-2014): $D_{IRR,m}$ (km^3)	
			Average monthly P-ET (2001-2017) for downstream cells with irrigation demand above threshold: $WA_{IRR,m}$ (km^3)	
	Industrial demand	$D_{IND,g}$	Average annual downstream industrial water use (2001-2014): $D_{IND,y}$ (km^3)	$\sum(D_{IND,m} - WA_{IND,m})/D_{IND,y}$
			Average monthly downstream industrial water use (2001-2014): $D_{IND,m}$ (km^3)	
			Average monthly P-ET (2001-2017) for downstream cells with industrial demand above threshold: $WA_{IND,m}$ (km^3)	
	Domestic demand	$D_{DOM,g}$	Average annual downstream domestic water use (2001-2014): $D_{DOM,y}$ (km^3)	$\sum(D_{DOM,m} - WA_{DOM,m})/D_{DOM,y}$
			Average monthly downstream domestic water use (2001-2014): $D_{DOM,m}$ (km^3)	
			Average monthly P-ET (2001-2017) for downstream cells with domestic demand above threshold: $WA_{DOM,m}$ (km^3)	

	Environmental flow requirement	$D_{EF,g}$	Average annual Environmental Flow Requirement at river basin outlet (2001-2014): $D_{EF,y}$ (km^3) Average monthly Environmental Flow Requirement at river basin outlet (2001-2014): $D_{EF,m}$ (km^3) Average monthly P-ET (2001-2017) for downstream subbasins: $WA_{EF,m}$ (km^3)	$\sum(D_{EF,m} - WA_{EF,m})/D_{EF,y}$
	Global Demand Index	DI_g	-	$(D_{IRR,g}+D_{IND,g}+D_{DOM,g}+D_{EF,g})/4$
Regional Demand Index	Irrigation demand	$D_{IRR,r}$	Average annual downstream irrigation water use (2001-2014): $D_{IRR,y}$ (km^3) Average monthly downstream irrigation water use (2001-2014): $D_{IRR,m}$ (km^3) Average monthly P-ET (2001-2017) for downstream cells with irrigation demand above threshold: $WA_{IRR,m}$ (km^3) Average monthly discharge for rWTUs (1961-2007): Q_{rWTU} (km^3)	$\sum(D_{IRR,m} - WA_{IRR,m} - Q_{rWTU})/D_{IRR,y}$
	Industrial demand	$D_{IND,r}$	Average annual downstream industrial water use (2001-2014): $D_{IND,y}$ (km^3) Average monthly downstream industrial water use (2001-2014): $D_{IND,m}$ (km^3)	$\sum(D_{IND,m} - WA_{IND,m} - Q_{rWTU})/D_{IND,y}$

Domestic demand	$D_{DOM,r}$	Average monthly P-ET (2001-2017) for downstream cells with industrial demand above threshold: $WA_{IND,m}$ (km^3) Average monthly discharge for rWTUs (1961-2007): Q_{rWTU} (km^3) Average annual downstream domestic water use (2001-2014): $D_{DOM,y}$ (km^3)	$\sum(D_{DOM,m} - WA_{DOM,m} - Q_{rWTU})/D_{DOM,y}$
Environmental flow requirement	$D_{EF,r}$	Average monthly downstream domestic water use (2001-2014): $D_{DOM,m}$ (km^3) Average monthly P-ET (2001-2017) for downstream cells with domestic demand above threshold: $WA_{DOM,m}$ (km^3) Average monthly discharge for rWTUs (1961-2007): Q_{rWTU} (km^3) Max annual Environmental Flow Requirement at river basin outlet (2001-2014): $D_{EF,y}$ (km^3)	$\sum(D_{EF,m} - WA_{EF,m} - Q_{rWTU})/D_{EF,y}$
Regional Demand Index	DI_r	Max monthly Environmental Flow Requirement at river basin outlet (2001-2014): $D_{EF,m}$ (km^3) Total monthly P-ET (2001-2017) for downstream subbasins: $WA_{EF,m}$ (km^3) Average monthly discharge for rWTUs (1961-2007): Q_{rWTU} (km^3) -	$(D_{IRR,r}+D_{IND,r}+D_{DOM,r}+D_{EF,r})/4$

Water Tower Index - global data	Regional Water Tower Index - global data	$rWTI_g$	-	$rWTI_g=SI_g*DI_g$
	Normalized regional Water Tower Index - global data	$rWTI_{nor,g}$	-	$rWTI_{nor,g}=(rWTI_g-min(rWTI_g)/max((rWTI_g)-min(rWTI_g))$
Water Tower Index - regional data	Regional Water Tower Index - regional data	$rWTI_r$	-	$rWTI_r=SI_r*DI_r$
	Normalized regional Water Tower Index - regional data	$rWTI_{nor,r}$	-	$rWTI_{nor,r}=(rWTI_r-min(rWTI_r)/max((rWTI_r)-min(rWTI_r))$

Annex IV

Table 7: Outcomes of the global WTI /VI and rWTI/VI, displaying the differences between these two approaches (Third column contains data from Immerzeel et al., 2020).

Section	Which indicator or sub-indicator	Indus Basin/WTU	Indus subbasin/ rWTU	Kabul	Kurram/ Tochi	Gumal	Jhelum	Chenab	Ravi	Beas/ Sutlej
Supply Index	Precipitation contribution to rWTU/subbasin (P_T)	0.71	0.695	0.545	0.339	0.102	0.593	0.519	0.240	0.605
	Interannual variability in precipitation (P_{YV})	0.70	0.670	0.668	0.685	0.492	0.684	0.607	0.651	0.622
	Intra-annual variability in precipitation (P_{MV})	0.25	0.301	0.318	0.162	0.119	0.221	0.173	0.115	0.074
	Precipitation (P)	0.34	0.337	0.269	0.144	0.031	0.269	0.203	0.092	0.211
	Annual snow cover (S_T)	0.33	0.412	0.271	0.048	0.018	0.273	0.410	0.234	0.287

	Interannual variability in snow cover (S_{YV})	0.16	0.710	0.636	0.175	0.019	0.650	0.710	0.537	0.438
	Intra-annual variability in snow cover (S_{MV})	0.67	0.216	0.077	0.004	0.001	0.047	0.225	0.138	0.117
	Snowmelt (S)	0.13	0.191	0.096	0.004	0.000	0.095	0.192	0.079	0.080
	Glacier ice storage (G_S)	0.87	0.997	0.983	0.000	0.000	0.876	0.993	0.953	0.980
	Glacier water yield (G_Y)	0.09	0.822	0.480	0.000	0.000	0.235	0.740	0.468	0.558
	Glacial melt (G)	0.48	0.910	0.732	0.000	0.000	0.556	0.867	0.711	0.769
	Surface waters (L)	0.22	0.268	0.015	0.006	0.000	0.003	0.008	0.229	0.413
	Supply Index (SI)	0.29	0.426	0.278	0.039	0.008	0.231	0.317	0.278	0.368
Demand Index	Irrigation demand (D_{IRR})	0.91	0.979	0.942	0.985	0.996	0.990	0.996	0.997	0.993
	Industrial demand (D_{IND})	0.69	0.758	0.697	0.860	0.936	0.817	0.866	0.893	0.820
	Domestic demand (D_{DOM})	0.59	0.680	0.586	0.818	0.907	0.705	0.845	0.905	0.801
	Environmental flow requirement (D_{EF})	0.84	0.071	0.077	0.125	0.118	0.061	0.087	0.123	0.049

	Demand Index (DI)	0.76	0.622	0.576	0.697	0.739	0.643	0.698	0.729	0.666
Regional Water Tower Index	rWTI (rWTI)	0.22	0.265	0.160	0.027	0.006	0.148	0.222	0.202	0.245
	rWTI normalized ($rWTI_{nor}$)	1.00	1.000	0.595	0.081	0.000	0.549	0.832	0.758	0.922
Vulnerability Index	Government effectiveness	-0.36	-0.268	-0.778	-0.649	-0.644	-0.482	-0.415	-0.493	-0.074
	Hydro-political tension	3	3	3	3	3	3	3	3	3
	Water Stress	2.2	1.611	1.658	1.951	2.317	2.947	3.077	3.369	3.359
	Mean dPop scaled	0.175	0.317	0.429	0.485	0.500	0.224	0.237	0.274	0.215
	Uncertainty to dPop	0.000	0.278	0.342	0.463	0.500	0.192	0.184	0.228	0.183
	Total indicator dPop	0.175	0.594	0.771	0.948	1.000	0.416	0.421	0.502	0.398
	Mean dGDP scaled	0.377	0.383	0.383	0.458	0.464	0.368	0.358	0.404	0.500
	Uncertainty to dGDP	0.000	0.275	0.297	0.261	0.253	0.327	0.336	0.334	0.500
	Total indicator dGDP	0.377	0.658	0.680	0.720	0.717	0.695	0.694	0.738	1.000
	Mean dP scaled	0.000	0.000	0.500	0.023	0.034	0.073	0.000	0,000	0.000
	Uncertainty to dP	0.000	0.162	0.294	0.489	0.435	0.258	0.268	0.293	0.168

Total indicator dP	0.000	0.162	0.794	0.513	0.469	0.331	0.268	0.293	0.168
Mean dT scaled	0.406	0.500	0.487	0.462	0.462	0.474	0.459	0.452	0.474
Uncertainty to dT	0.000	0.424	0.400	0.474	0.440	0.417	0.500	0.488	0.376
Total indicator dT	0.406	0.924	0.887	0.936	0.902	0.891	0.959	0.941	0.850

Table 8: Overview of the not scaled values of the dPop, dGDP, dP and dT indicators for global data, of which the scaled values are given in Table 7.

		Indus Basin/ WTU	Indus subbasin/ rWTU	Kabul	Kurram/ Tochi	Gumal	Jhelum	Chenab	Ravi	Beas/ Sutlej
dPop SSP1	dPop 2000-2050 (%)	-	59.631	85.711	89.379	87.421	44.158	50.445	56.951	42.266
	Uncertainty to dPop (%)	-	31.291	37.500	49.961	56.182	20.281	17.601	21.709	19.598
dPop SSP3	dPop 2000-2050 (%)	-	129.445	171.760	206.295	213.083	92.691	97.407	115.117	88.368
	Uncertainty to dPop (%)	-	38.523	48.549	66.955	69.480	28.251	29.360	36.457	26.504
dPop SSP2	Mean dPop SSP2 2000-2050 (%)	50.305	90.922	123.211	139.341	143.603	64.440	68.047	78.660	61.864
	Mean uncertainty to dPop (%)	-	34.907	43.024	58.458	62.831	24.266	23.481	29.083	23.051
dGDP SSP1	dGDP 2000-2050 (%)	-	985.699	1051.600	1113.826	1103.201	1023.976	1037.094	1131.626	1492.940
	Uncertainty to dGDP (%)	-	204.581	270.475	179.783	157.491	274.501	307.506	307.290	473.367
dGDP SSP3	dGDP 2000-2050 (%)	-	533.025	552.036	686.835	693.377	478.924	472.236	569.660	648.443
	Uncertainty to dGDP (%)	-	248.093	229.089	247.208	252.334	270.551	257.352	254.675	371.129
dGDP SSP2	Mean dGDP SSP2 2000-2050 (%)	769.228	781.117	781.125	934.044	945.711	749.475	729.588	824.336	1019.573
	Mean uncertainty to dGDP (%)	-	226.337	249.782	213.496	204.912	272.526	282.429	280.983	422.248

		Indus Basin/ WTU	Indus subbasin/ rWTU	Kabul	Kurram/ Tochi	Gumal	Jhelum	Chenab	Ravi	Beas/ Sutlej
dP RCP 4.5	Mean dP (%)	0.236	1.211	-3.019	-0.284	-0.416	-0.878	1.162	1.067	2.021
	Uncertainty to dP (%)	-	-12.854	-18.979	-34.425	-25.418	-16.418	-18.851	-19.229	-13.360
dP RCP 8.5	Mean dP (%)	-	3.374	-1.669	3.427	3.428	1.106	3.743	4.470	3.829
	Uncertainty to dP (%)	-	-10.598	-24.057	-36.950	-38.629	-21.471	-20.259	-23.748	-10.927
dP Mean of RCPs	Mean dP (%)	-	2.293	-2.344	1.571	1.506	0.114	2.452	2.768	2.925
	Uncertainty to dP (%)	-	-11.726	-21.518	-35.688	-32.024	-18.945	-19.555	-21.489	-12.144
dT RCP 4.5	Mean dT (˚C)	1.878	1.932	1.878	1.786	1.785	1.824	1.767	1.735	1.829
	Uncertainty to dT (˚C)	-	1.271	1.066	1.325	1.279	0.990	1.348	1.325	0.987
dT RCP 8.5	Mean dT (˚C)	-	2.692	2.623	2.485	2.483	2.557	2.484	2.454	2.559
	Uncertainty to dT (˚C)	-	1.225	1.319	1.483	1.323	1.522	1.627	1.578	1.256
dT Mean of RCPs	Mean dT (˚C)	-	2.312	2.251	2.136	2.134	2.191	2.125	2.094	2.194
	Uncertainty to dT (˚C)	-	1.248	1.193	1.404	1.301	1.256	1.488	1.451	1.121

Annex V

Table 9: Outcomes of the rWTI and VI for global and regional data. Per indicator, there are two rows: the first row indicates the outcome using the global approach, while the second row indicates the outcome using the regional approach.

Which section	Which indicator or sub-indicator	Indus subbasin/ rWTU	Kabul	Kurram/ Tochi	Gumal	Jhelum	Chenab	Ravi	Beas/ Sutlej
Supply Index	Interannual variability snow (S_{YV})	0.710	0.636	0.175	0.019	0.650	0.710	0.537	0.438
		0.178	0.118	0.000	0.000	0.003	0.065	0.047	0.243
	Intra-annual variability snow (S_{MV})	0.216	0.077	0.004	0.001	0.047	0.225	0.138	0.117
		0.022	0.010	0.000	0.000	0.000	0.003	0.004	0.027
	Snowmelt (S)	0.191	0.096	0.004	0.000	0.095	0.192	0.079	0.080
		0.029	0.042	0.000	0.000	0.001	0.012	0.004	0.037
	Glacier ice storage (G_s) / Interannual variability glacier (G_{YV})	0.997	0.983	0.000	0.000	0.876	0.993	0.953	0.980
		0.411	0.629	0.000	0.000	1.000	1.000	0.594	0.602
	Glacier water yield (G_Y) /	0.822	0.480	0.000	0.000	0.235	0.740	0.468	0.558
		0.001	0.001	0.000	0.000	1.000	1.000	0.001	0.001

	Intra-annual variability glacier (G_{MV})								
	Glacial melt (G)	0.910	0.732	0.000	0.000	0.556	0.867	0.711	0.769
		0.062	0.028	0.000	0.000	0.002	0.170	0.001	0.006
	Surface waters (L)	0.268	0.015	0.006	0.000	0.003	0.008	0.229	0.413
		0.267	0.015	0.006	0.000	0.003	0.008	0.229	0.413
	Supply Index (SI)	0.426	0.278	0.039	0.008	0.231	0.317	0.278	0.368
		0.174	0.089	0.037	0.008	0.069	0.098	0.082	0.166
Demand Index	Irrigation demand (D_{IRR})	0.979	0.942	0.985	0.996	0.990	0.996	0.997	0.993
		0.448	0.644	0.218	0.264	0.542	0.602	0.656	0.781
	Industrial demand (D_{IND})	0.758	0.697	0.860	0.936	0.817	0.866	0.893	0.820
		0.025	0.128	0.000	0.007	0.163	0.268	0.514	0.603
	Domestic demand (D_{DOM})	0.680	0.586	0.818	0.907	0.705	0.845	0.905	0.801
		0.021	0.104	0.000	0.016	0.139	0.291	0.522	0.578
	Environmental flow requirement (D_{EF})	0.071	0.077	0.125	0.118	0.061	0.087	0.123	0.049
		0.000	0.000	0.000	0.000	0.000	0.000	0.000	0.000
	Demand Index (DI)	0.622	0.576	0.697	0.739	0.643	0.698	0.729	0.666
		0.124	0.219	0.055	0.072	0.211	0.290	0.423	0.491
Regional Water Tower Index	rWTI (rWTI)	0.265	0.160	0.027	0.006	0.148	0.222	0.202	0.245
		0.021	0.019	0.002	0.001	0.014	0.028	0.034	0.082

	rWTI normalized	1.000	0.595	0.081	0.000	0.549	0.832	0.758	0.922
	($rWTI_{nor}$)	0.258	0.232	0.018	0.000	0.171	0.344	0.419	1.000
Vulnerability Index	Hydro-political tension	3	3	3	3	3	3	3	3
		5	2	3	2	5	5	3	3
	Government effectiveness	-0.268	-0.778	-0.649	-0.644	-0.482	-0.415	-0.493	-0.074
		-0.292	-0.883	-0.745	-0.740	-0.548	-0.464	-0.562	-0.051
	Water Stress	0.000	0.026	0.193	0.402	0.760	0.834	1.000	0.994
		0.531	0.230	0.040	0.000	0.031	0.023	0.066	1.000
	Mean dPop scaled	0.325	0.437	0.489	0.500	0.240	0.264	0.293	0.223
		0.429	0.500	0.234	0.266	0.397	0.415	0.457	0.346
	Uncertainty to dPop	0.306	0.354	0.467	0.500	0.226	0.218	0.260	0.215
		0.366	0.410	0.439	0.500	0.365	0.392	0.384	0.334
	Total indicator dPop	0.631	0.791	0.956	1.000	0.466	0.482	0.554	0.438
		0.796	0.910	0.673	0.766	0.762	0.807	0.840	0.679
	Mean dGDP scaled	0.420	0.452	0.497	0.500	0.371	0.380	0.408	0.395
		0.440	0.461	0.344	0.363	0.462	0.443	0.482	0.500
	Uncertainty to dGDP	0.366	0.418	0.338	0.325	0.411	0.441	0.414	0.500
		0.323	0.257	0.134	0.145	0.390	0.315	0.466	0.359
	Total indicator dGDP	0.786	0.870	0.836	0.825	0.782	0.821	0.822	0.895
		0.764	0.718	0.479	0.508	0.851	0.758	0.947	0.859
	Mean dP scaled	0.000	0.500	0.023	0.034	0.073	0.000	0.000	0.000
		0.000	0.452	0.500	NA	0.177	0.000	0.000	0.000
	Uncertainty to dP	0.162	0.294	0.489	0.435	0.258	0.268	0.293	0.168

	0.352	0.459	0.500	NA	0.441	0.461	0.497	0.395
Total indicator dP	0.162	0.794	0.513	0.469	0.331	0.268	0.293	0.168
	0.352	0.911	1.000	NA	0.618	0.461	0.497	0.395
Mean dT scaled	0.500	0.487	0.462	0.462	0.474	0.459	0.452	0.474
	0.500	0.484	0.477	NA	0.482	0.458	0.449	0.463
Uncertainty to dT	0.424	0.400	0.474	0.440	0.417	0.500	0.488	0.376
	0.478	0.458	0.413	NA	0.436	0.422	0.419	0.457
Total indicator dT	0.924	0.887	0.936	0.902	0.891	0.959	0.941	0.850
	0.978	0.942	0.890	NA	0.918	0.880	0.868	0.920

Table 10: Overview of the not scaled values of water stress, dPop, dGDP, dP and dT indicators for regional data, of which the scaled values are given in Table 9. Per indicator, there are two rows: the first row indicates the outcome using the global approach, while the second row indicates the outcome using the regional approach.

		Indus subbasin/ rWTU	**Kabul**	**Kurram/ Tochi**	**Gumal**	**Jhelum**	**Chenab**	**Ravi**	**Beas/ Sutlej**
Water Stress	Baseline Water Stress	1.611	1.658	1.951	2.317	2.947	3.077	3.369	3.359
	Unsustainable groundwater extraction (km^3)	2877	1295	296	83.1	248	205	432	5341
		Indus subbasin/ rWTU	**Kabul**	**Kurram/ Tochi**	**Gumal**	**Jhelum**	**Chenab**	**Ravi**	**Beas/ Sutlej**
dPop SSP1/ Downhill	dPop 2016-2050 (%)	18.427 87.626	29.770 103.411	28.685 62.317	26.212 71.909	14.563 83.025	19.829 86.831	20.860 96.810	13.005 70.242
	Uncertainty to dPop (%)	23.214 27.210	26.204 33.076	33.949 29.342	37.834 34.557	16.118 27.164	14.019 28.427	16.717 32.540	15.567 21.607
dPop SSP3/P rosperous	dPop 2016-2050 (%)	70.220 34.461	89.898 49.799	108.131 8.807	110.834 6.551	53.132 30.024	57.233 28.290	65.651 50.324	49.625 14.586
	Uncertainty to dPop (%)	28.579 53.165	33.925 53.613	45.496 71.124	46.789 78.461	22.451 53.000	23.385 58.541	28.074 46.485	21.053 55.657
dPop SSP2/B usiness as Usual	Mean dPop BAU 2016-2050 (%)	41.641 60.416	55.973 70.335	62.634 32.974	64.046 37.353	30.681 55.861	33.848 58.404	37.577 64.269	28.572 48.635
	Mean uncertainty to dPop (%)	25.897 40.187	30.064 43.344	39.723 50.233	42.311 56.509	19.284 40.082	18.702 43.484	22.396 39.513	18.310 38.632
dGDP SSP1/	dGDP 2016-2050 (%)	418.744 266.312	482.349 383.787	464.083 233.424	455.220 238.337	407.545 284.166	435.928 267.832	448.867 297.565	472.032 288.841

Downhill	Uncertainty to dGDP (%)	97.748 157.200	136.776 59.634	83.548 97.749	72.674 110.718	123.954 159.848	144.932 157.778	136.942 165.563	169.988 191.894
dGDP SSP3/Prosperous	dGDP 2016-2050 (%)	202.458 542.508	229.726 622.860	265.654 338.303	266.106 348.617	161.420 625.834	169.702 535.705	198.431 713.890	168.769 590.131
	Uncertainty to dGDP (%)	118.538 118.997	115.847 179.439	114.881 7.130	116.440 0.438	122.171 181.820	121.294 110.095	113.495 250.762	133.274 109.396
dGDP SSP2/Business as Usual	Mean dGDP BAU 2016-2050 (%)	320.996 423.511	345.573 443.421	380.536 331.172	382.546 349.055	283.591 444.013	290.996 425.610	311.925 463.128	302.044 480.735
	Mean uncertainty to dGDP (%)	108.143 138.098	126.311 119.537	99.215 52.440	94.557 55.578	123.063 170.834	133.113 133.936	125.218 208.162	151.631 150.645
		Indus subbasin/ rWTU	**Kabul**	**Kurram/ Tochi**	**Gumal**	**Jhelum**	**Chenab**	**Ravi**	**Beas/ Sutlej**
dP RCP 4.5	Mean dP (%)	1.211 -1.758	-3.019 -7.712	-0.284 -6.883	-0.416 NA	-0.878 -8.145	1.162 -2.975	1.067 -1.123	2.021 2.986
	Uncertainty to dP (%)	-12.854 -5.422	-18.979 -11.435	-34.425 -15.219	-25.418 NA	-16.418 -5.465	-18.851 -5.388	-19.229 -4.706	-13.360 -4.844
dP RCP 8.5	Mean dP (%)	3.374 10.688	-1.669 -3.001	3.427 -4.964	3.428 NA	1.106 3.940	3.743 11.120	4.470 15.340	3.829 18.511
	Uncertainty to dP (%)	-10.598 -22.844	-24.057 -25.395	-36.950 -24.928	-38.629 NA	-21.471 -29.945	-20.259 -31.628	-23.748 -35.213	-10.927 -26.882
dP Mean of RCPs	Mean dP (%)	2.293 4.465	-2.344 -5.357	1.571 -5.923	1.506 NA	0.114 -2.102	2.452 4.073	2.768 7.109	2.925 10.749
	Uncertainty to dP (%)	-11.726 -14.133	-21.518 -18.415	-35.688 -20.074	-32.024 NA	-18.945 -17.705	-19.555 -18.508	-21.489 -19.959	-12.144 -15.863
dT RCP	Mean dT (˚C)	1.932 3.274	1.878 3.211	1.786 3.140	1.785 NA	1.824 3.201	1.767 2.997	1.735 2.926	1.829 2.986

4.5	Uncertainty to dT (˚C)	1.271 1.184	1.066 1.153	1.325 1.058	1.279 NA	0.990 1.177	1.348 1.048	1.325 0.964	0.987 0.982
dT RCP 8.5	Mean dT (˚C)	2.692 6.308	2.623 6.020	2.485 5.985	2.483 NA	2.557 5.991	2.484 5.772	2.454 5.692	2.559 5.927
	Uncertainty to dT (˚C)	1.225 1.205	1.319 1.132	1.483 1.000	1.323 NA	1.522 0.989	1.627 1.062	1.578 1.139	1.256 1.321
dT Mean of RCPs	Mean dT (˚C)	2.312 4.791	2.251 4.616	2.136 4.562	2.134 NA	2.191 4.596	2.125 4.384	2.094 4.309	2.194 4.456
	Uncertainty to dT (˚C)	1.248 1.194	1.193 1.143	1.404 1.029	1.301 NA	1.256 1.083	1.488 1.055	1.451 1.051	1.121 1.151